

1 Dear dr. Aninda Mazumdar and dr. Andrew Johnson,

2

3 On behalf of all authors, I would like to thank you for your additional comments on our
4 manuscript. We are glad to receive a positive reply to our revisions of the manuscript and are
5 happy to implement the additional minor revisions to the text to ready our manuscript for
6 publication. Please find our point-by-point rebuttal (in red) to these suggestions below, including
7 details on how we implement the necessary changes to the text, where applicable.

8

9 *Associate Editor Decision: Publish subject to minor revisions (review by editor) (14 Apr 2020) by*
10 *Aninda Mazumdar*

11 *Dear Authors,*

12 *Kindly go through the comments from the reviewer and submit the revised manuscript for a final*
13 *decision. You have made substantial improvement in the text, however some clarity is required*
14 *at few places as mentioned by the reviewer.*

15 *sincerely*

16 *Aninda Mazumdar*

17

18 *Thank you for your moderation of the review process and for giving us the opportunity to*
19 *respond to these and previous review comments. We are looking forward to hearing your*
20 *decision.*

21

22 *Suggestions for revision Referee #4 (dr. Andrew Johnson)*

23 *The authors have responded very positively to comments: the paper now has a clear 'thread'*
24 *and is therefore much easier to read and appreciate. The results and conclusions are novel and*
25 *important, and certainly merit publication. I have made a number of corrections and comments*
26 *(in square brackets) in the annotated version of the manuscript supplied alongside. Most will be*
27 *straightforward to address but the authors need to give a little more time to sections 5.5.2 and*
28 *5.5.3. Although I finally worked out what the authors were saying about spawning in section*
29 *5.5.2 (I had misunderstood their application of the term as spawning BY the individuals*
30 *investigated), some clarification of the text to prevent similar misunderstanding by other readers,*
31 *together with reconsideration/correction of other points in this and the next section (5.5.3), are*
32 *needed. Once these issues (and additional minor points) have been addressed the paper will be*
33 *ready for publication, and it will be an excellent contribution to the literature.*

34

35 *We are glad to hear that dr. Johnson considers the manuscript improved, and are very happy*
36 *with his feedback that helped us to better structure our manuscript and clarify our discussion.*

37 *We regret that our discussion in section 5.5.2 was not clear and that we did not realize the*
38 *source of this confusion in our previous round of revisions. We will follow dr. Johnson's*

39 suggestions to prevent the same confusion from occurring with our future readers. We kindly
40 refer to the point by point rebuttal below regarding the other minor points raised by the reviewer.

41

42 **Minor in-text comments**

43 Line 29: “complement” changed to “complements”

44 Line 34: “allows” changed to “allow”

45 Line 40-41: These statements do not contrast

46 Correct, we rephrase to clarify that the “latitudinal gradients similar to the present” contrast with
47 the notion of “equable climate”

48 Line 68: “land ice free” rephrased to “essentially land-ice free”

49 Line 76: “risk being seasonally biased” rephrased to “risk seasonal bias”

50 Line 131: “these” was deleted

51 Line 163: Line break was inserted after “2.5 Aim”

52 Line 198: “on” rephrased to “at”

53 Line 210: The yellow area in the centre of the image is within the valve. We replace “between”
54 with “within”

55 Line 218: “Germany).” Dot added to sentence

56 Line 228: ‘Regions of Interest’ Quotation marks were added

57 Line 230: “selection” rephrased to “formulation”

58 Line 236: “as” rephrased to “so as”

59 Line 280: “sampled” rephrased to “extracted”

60 Line 324: “were” was added between “samples” and “placed”

61 Line 395: “as it does in” rephrased to “to”

62 Line 396: “From this extrapolation” rephrased to “On this basis”

63 Line 396: “...shell height from microstructural...” rephrased to “...shell height at specific times in
64 ontogeny from microstructural...”

65 Line 399: “analyses” was removed

66 Line 409: “diagenetic” rephrased to “diagenetically altered”

67 Line 434: “are” rephrased to “were”

68 Line 435: “5point” rephrased to “5-point”

69 Line 442: Use one scale of comparison - lower/higher or lighter/heavier. Strictly speaking a
70 value can't be light/heavy so low/high is better.

71 Agreed, we now use “lower” and “higher”

72 Line 474: “predictable” rephrased to “widely-shared”

73 Line 507: “variety” rephrased to “variation”

74 Line 521: “in this integrated stratigraphic framework” was deleted

75 Line 525-528: Repetition of material in section 4.1 - try at least to minimise. Also, replace
76 'subdivision' with 'boundary'.

77 Agreed, we shortened this section to “Strontium isotope dating places the Ivö Klack deposits at
78 78.14 ± 0.26 Ma (Fig. 4), slightly above the early/late Campanian boundary. When plotting the
79 obtained age of 78.14 Ma on the compilation by Wendler (2013), the age of the Ivö Klack falls
80 slightly above the early/late Campanian subdivision (which is placed at ~ 78.5 Ma), while the B.
81 *mammilatus* biozone is defined as late early Campanian (Wendler, 2013).”

82 Line 566: “the results of this stud.” Rephrased to “our results for these element ratios”

83 Line 569: “likely” rephrased to “promising”

84 Line 572: “as basis” rephrased to “as a basis”

85 Line 580: “composition” rephrased to “content”

86 Line 582: “twice as low as in” rephrased to “half those of”

87 Line 583: “for example” was deleted

88 Line 583-584: “twice as low as” rephrased to “half”

89 Line 585: “remains” rephrased to “has remained”

90 Line 587: “entail” rephrased to “mean”

91 Line 587: “...fixed physiological limit to oyster’s discrimination against building Sr into their
92 shells ...” rephrased to “...physiologically fixed concentration of Sr in an oyster’s shell...”

93 Line 587: “building” rephrased to “incorporating”

94 Line 588: If a similar amount of Sr is incorporated when the ambient concentration is lower,
95 doesn’t it mean that the organism is still discriminating? Clarification needed.

96 Corrent, we rephrased this sentence clarifying that we hypothesize a fixed concentration of Sr in
97 oyster shells which is independent of the ambient seawater concentration (see comment on line
98 587).

99 Line 604: “(Fig. 6)” was added

100 Line 619: “values can be considerably lighter” rephrased to “values can be considerably lower”

101 Line 624: “...analyses (which does...)” Both either singular or plural.

102 Correct, this was rephrased to “...analyses (which do...)”

103 Line 625: “which” was deleted

104 Line 635: "based on" rephrased to "from"

105 Line 638: "paleolatitude" was deleted

106 Line 644: for Ivö Klack material. Not necessarily from this site, we rephrase to "independent
107 marine temperature proxies" to clarify

108 Line 652: "such" was deleted

109 Line 653: "In addition" rephrased to "In this respect it is important to recognise that"

110 Line 657-658: Better expressed as winter minimum and summer maximum temperatures for
111 clarity, with the median added for comparison with Ivö Klack MAT (almost the same parameter).
112 Omit mention of mean annual SST because you don't actually supply it.

113 Agreed, we rephrased this sentence referring to "seasonal SST range" rather than MAT.

114 Line 660: maximum seasonal range in temperature [+ cite source].

115 This was rephrased accordingly. The source is the same as in the previous sentence.

116 Line 662: "seasonality rephrased to "temperature seasonality"

117 Line 663: "those" was deleted

118 Line 663: "vs." rephrased to "and"

119 Line 663: "C respectively" added ", " between "C" and "respectively"

120 Line 671: "(2015).5.5 Shell growth and ontogeny" added line break before "5.5"

121 Line 679: "Von" rephrased to "von"

122 Line 686: "Von" rephrased to "von"

123 Line 687: "Ivö Klack cemented" added ", " between "Klack" and "cemented"

124 Line 688-689: As before, I find this obscure. Why not conclude the sentence by saying 'such
125 that individuals received the same (high) supply of food.'

126 A good suggestion, we replaced "but with little competition for space due to the high-energy
127 environment" with "such that individuals received the same (high) supply of food" to the end of
128 the sentence.

129 Line 693: "growth" rephrased to "growth curve"

130 Line 694: "K -value" deleted the space between "K" and "-value"

131 Line 699: "more unfavorable or restricting" Not sure if there is much difference (and one
132 wouldn't say that shallow settings are 'less unfavourable'). Why not substitute 'less favourable'
133 for both, which would also avoid confusion over what 'former group' refers to?

134 We thank dr. Johnson for this suggestion and rephrased "more unfavorable or restricting" with
135 "less favorable"

136 Line 704: "Von" rephrased to "von"

137 Line 710: "on" rephrased to "at"

138 Line 712-714: I think the authors are referring to the spawning which gave rise to each
139 individual. If so, say 'shows when the individual was spawned' to distinguish from its production
140 of spawn

141 We thank dr. Johnson for pointing this out. Indeed, we should have considered the time span
142 between spawning and settling in our discussion. We revised this part of the discussion to take
143 this into account. In the light of this and following comments, we rephrased "in which season
144 spawning occurred" to "in which season the individual settled and started growing its shell". We
145 edit this in the labels of Figure 11 too.

146 Line 719: "on" replaced by "at"

147 Line 719: Broadly, but you need to take into account the larval stage - see comment below. I
148 suggest you say first growth corresponds to 'time of post-larval settlement'

149 See above, we rephrase this to "coincides with the time of first growth at post-larval settlement"

150 Line 721: "(spawning)" rephrased to "(following settlement after the larval stage)"

151 Line 721: Surely you mean high d18O

152 Absolutely, we correct this mistake in the revised version.

153 Line 725: There is only one. Maybe 0.403 needs to be in green because you say 'significantly
154 influences' at L754. Make title of this column 'Length of growth season'.

155 We implement these changes in the table

156 Line 729: "stops" rephrased to "stopped"

157 Line 730: "are" rephrased to "were"

158 Line 731: "would be" rephrased to "had been"

159 Line 733: "should positively correlate" rephrased to "would have positively correlated"

160 Line 744: Implies that 'temperature of first growth' is not time of spawning - some modifications
161 needed to take into account the length of the larval stage

162 Correct, see our reply to previous comments. We take this in account while revising this part of
163 the discussion.

164 Line 745: "in" was removed

165 Line 746: "temperatures" rephrased to "temperature"

166 Line 756: "extent" rephrased to "range"

167 Line 762-763: Maybe they correspond to attempted predation

168 This is an interesting hypothesis and we add it here as a tentative explanation.

169 Line 765: Oysters can tolerate lower temperatures than this. I think you may mean the lowest
170 temp. at which growth occurs.

171 Correct, we rephrase this to "...the lower (~10°C) nor the upper temperature limit of temperature
172 tolerance (~28°C) between which shell growth occurs..."

173 Line 767-768: "mild seasonal temperature cycle" rephrased to "mild seasonal temperatures"

174 Line 773: You have identified the season of spawning as winter in Fig.11b. Actually this is the
175 time of settlement so you really can't say that spawning was in spring.

176 Correct, we revise the discussion in this paragraph accordingly

177 Line 778: It's not clear why. Spring is not a time of max. or min. temperature.

178 We clarify this by explaining that the input of freshwater dampens the seasonal cycle in $\delta^{18}\text{O}$:
179 "...while also dampening the reconstructed temperature seasonality reconstructed from $\delta^{18}\text{O}$
180 due to the influx of isotopically light fresh water which dampens the seasonal cycle..."

181 Line 787: "season" replaced by "year"

182 Line 795-796: OK, but note indirect temperature effects (doi:10.1007/s12237-010-9267-4) and
183 effects of feeding rate and food type (doi:10.1016/j.gca.2015.07.010) on $\delta^{13}\text{C}$

184 We thank dr. Johnson for the suggested references and added them to this part of the
185 discussion about carbon isotope ratios in bivalve shells.

186 Line 799-800: Neither are the low d18O season

187 Agreed, we made the same mistake as in line 721. This has been rephrased to "high-d18O
188 season" in the revised text.

189 Line 800: See comment at L773 re the timing of spawning

190 Correct, this has been rephrased to "settling of larvae and the onset of shell growth"

191 Line 812: "and" rephrased to "but"

192 Line 813: "trends in *R. diluvianum*" rephrased to "trends is inconsistent in *R. diluvianum*"

193 Line 816: "on" rephrased to "at"

194 Line 824: "from limited" rephrased to "from the limited"

195 Line 844: "argue" rephrased to "argues"

196 Line 849: "disadvantage of the lack of" rephrased to "need for more"

197 Line 850: "such reconstructions" rephrased to "such proxy-based reconstructions"

198 Line 855: "However, changes..." rephrased to "However, ontogenetic changes"

199 Line 875: "with combining" rephrased to "in handling"

200

201 **Please find our annotated manuscript below:**

202 **Shell chemistry of the Boreal Campanian bivalve *Rastellum diluvianum* (Linnaeus,**
203 **1767) reveals temperature seasonality, growth rates and life cycle of an extinct**
204 **Cretaceous oyster.**

205 Niels J. de Winter^{1*}, Clemens V. Ullmann², Anne M. Sørensen³, Nicolas Thibault⁴, Steven
206 Goderis¹, Stijn J.M. Van Malderen⁵, Christophe Snoeck^{1,6}, Stijn Goolaerts⁷, Frank Vanhaecke⁵,
207 Philippe Claeys¹

Formatted: Not Superscript/ Subscript

208

209 ¹AMGC research group, Vrije Universiteit Brussel, Pleinlaan 2, B-1050 Brussels, Belgium.

210 ²Camborne School of Mines, University of Exeter, Penryn, Cornwall, TR10 9FE, UK.

211 ³Trap Danmark, Agem All 13, DK-2970, Hørsholm, Denmark.

212 ⁴ Department of Geoscience and Natural Resource Management, University of Copenhagen,
213 Øster Voldgade 10, DK-1350 Copenhagen C., Denmark.

214 ⁵A&MS research unit, Ghent University Campus Sterre, Krijgslaan 281, Building S12, B-9000
215 Ghent, Belgium.

216 ⁶G-Time laboratory, Université Libre de Bruxelles, 50 Avenue F.D. Roosevelt, B-1050, Brussels,
217 Belgium.

218 ⁷Directorate of Earth and History of Life, Royal Belgian Institute of Natural Sciences, Vautierstraat
219 29, B-1000 Brussels, Belgium.

220 [*Now at: Department of Earth Sciences, Faculty of Geosciences, Utrecht University, the](#)
221 [Netherlands](#)

222

223 Correspondence to: Niels J. de Winter (niels.de.winter@vub.be)

224

225

226 **Abstract**

227 The Campanian age (Late Cretaceous) is characterized by a warm greenhouse climate with limited land
228 ice volume. This makes this period an ideal target for studying climate dynamics during greenhouse periods,
229 which are essential for predictions of future climate change due to anthropogenic greenhouse gas
230 emissions. Well-preserved fossil shells from the Campanian (± 78 Ma) high mid-latitude (50°N) coastal
231 faunas of the Kristianstad Basin (southern Sweden) offer a unique snapshot of short-term climate and
232 environmental variability, which complements existing long-term climate reconstructions. In this study, we
233 apply a combination of high-resolution spatially resolved trace element analyses (μ XRF and LA-ICP-MS),
234 stable isotope analyses (IRMS) and growth modelling to study short-term (seasonal) variations recorded in
235 the oyster species *Rastellum diluvianum* from the Ivö Klack locality. Geochemical records through 12
236 specimens shed light on the influence of specimen-specific and ontogenetic effects on the expression of
237 seasonal variations in shell chemistry and allows disentangling vital effects from environmental influences
238 in an effort to refine palaeoseasonality reconstructions of Late Cretaceous greenhouse climates. Growth
239 models based on stable oxygen isotope records yield information on the mode of life, circadian rhythm and
240 reproductive cycle of these extinct oysters. This multi-proxy study reveals that mean annual temperatures
241 in the Campanian higher mid-latitudes were 17 to 19°C with winter minima of $\sim 13^\circ\text{C}$ and summer maxima
242 of 26°C , assuming a Late Cretaceous seawater oxygen isotope composition of -1‰ VSMOW . These results
243 yield smaller latitudinal differences in temperature seasonality in the Campanian compared to today.
244 latitudinal-Latitudinal temperature gradients were similar to the present, but with smaller latitudinal
245 differences in temperature seasonality, contrasting with previous notions of “equable climate” during the
246 Late Cretaceous. Our results also demonstrate that species-specific differences and uncertainties in the
247 composition of Late Cretaceous seawater prevent trace element proxies (Mg/Ca, Sr/Ca, Mg/Li and Sr/Li)
248 to be used as reliable temperature proxies for fossil oyster shells. However, trace element profiles can serve
249 as a quick tool for diagenesis screening and investigating seasonal growth patterns in ancient shells.

250

251 **1. Introduction**

252 The Late Cretaceous was marked by a long cooling trend that brought global mean annual temperatures
253 (MAT) down from the mid-Cretaceous climate maximum ($\pm 28^{\circ}\text{C}$ surface ocean temperatures) in the
254 Cenomanian and Turonian (± 95 Ma) to slightly cooler temperatures ($\pm 22^{\circ}\text{C}$ surface ocean temperatures)
255 around the Campanian-Maastrichtian boundary (± 72.1 Ma; Clarke and Jenkyns, 1999; Pearson et al., 2001;
256 Huber et al., 2002; Friedrich et al., 2012; Scotese, 2016). This cooling trend was likely caused by a change
257 in ocean circulation, initiated by the opening of the Equatorial Atlantic Gateway that separated the proto-
258 North and -South Atlantic Ocean basins (Friedrich et al., 2009). The cooling trend is well documented in
259 stable oxygen isotope records from the white chalk successions of the Chalk Sea, which covered large
260 portions of northwestern Europe during the Late Cretaceous Period (Reid, 1973; Jenkyns et al., 1994; Jarvis
261 et al., 2002; Voigt et al., 2010). The connection of the Chalk Sea to the (proto-)North Atlantic Ocean makes
262 it an interesting area of study to constrain Late Cretaceous paleogeography and climate. These chalk
263 successions featured in various paleoclimate studies, because they are accessible in good outcrops and
264 consist predominantly of calcareous nanofossils which were thought to faithfully record sea surface
265 conditions (e.g. Jenkyns et al., 1994). However, recent studies (e.g. O'Brien et al., 2017; Tagliavento et al.,
266 2019) have shown that diagenetic overprinting likely biases these records towards cooler temperatures,
267 resulting in the apparent Cool Tropics Paradox (Pearson et al., 2001). Even though sea level changes seem
268 to indicate possible small changes in land ice volume during the Late Cretaceous, warm high-latitude
269 paleotemperatures likely rule out the possibility of extensive polar ice sheets comparable in volume to
270 modern ice caps (Barrera and Johnson, 1999; Huber et al., 2002; Jenkyns et al., 2004; Miller et al., 2005;
271 Thibault et al., 2016).

272 Given its warm, essentially land-ice free conditions, the Campanian serves as an interesting analogue for
273 Earth's climate in the future, should anthropogenic and natural emissions continue to contribute to the rise
274 in global temperatures and decrease global ice volume on Earth (IPCC, 2013; Donnadieu et al., 2016).
275 However, most Late Cretaceous climate reconstructions focus on reconstructing and modelling long-term
276 evolutions of humid/arid conditions on land or past atmospheric and oceanic temperatures (DeConto et al.,
277 1999; Thibault et al., 2016; Yang et al., 2018). Data on the extent of seasonal variability from this time
278 period, especially outside the tropics, are scarce, although seasonality constitutes a fundamental
279 component of the climate system (Steuber, 1999; Steuber et al., 2005; Burgener et al., 2018). Furthermore,

280 many proxies used for paleoclimate reconstruction risk ~~being seasonally biased~~seasonal bias, and thus
281 independent seasonality reconstructions serve as important tools to verify other climate reconstructions.

282

283 **2. Background**

284 **2.1 Geological setting**

285 The Kristianstad Basin, our study site, is located on the southeastern Baltic Sea coast of the southern
286 Swedish province of Skåne, which is presently located at 56°2' N, 14° 9' E (see **Fig. 1**), somewhat higher
287 than its Campanian paleolatitude, which is estimated at 50°N (van Hinsbergen et al., 2015). The uppermost
288 lower Campanian shallow marine sediments deposited at Ivö Klack consist of sandy and silty nearshore
289 deposits containing carbonate gravel (Christensen, 1975; 1984; Surlyk and Sørensen, 2010; Sørensen et
290 al., 2015). The depositional setting is described as a rocky coastline that was inundated during the
291 maximum extent of the Late Cretaceous transgression (Kominz et al., 2008; Csiki-Sava et al., 2015). Since
292 the region has remained tectonically quiet since the Campanian, the deposits of Kristianstad Basin localities
293 remain at roughly the same altitude as when they were deposited and have been subject to limited burial
294 (Christensen, 1984; Surlyk and Sørensen, 2010).

295 The rocky shore deposits of Ivö Klack are characterized by a diverse shelly fauna, consisting of well-
296 preserved fossils and fragments of brachiopods, belemnites, echinoids and asteroids, polychaete worms,
297 gastropods, corals, ammonites and thick-shelled oysters, with a total of almost 200 different recognized
298 species (Surlyk and Sørensen, 2010). In this diverse rocky shore ecosystem, various habitat zones can be
299 distinguished, each with their distinct suite of organisms adapted to local conditions of varying amounts of
300 sunlight, sedimentation and turbulence (Surlyk and Christensen, 1974; Sørensen et al., 2012). This unique
301 combination of marine biodiversity and preservation of original calcite shell material makes the localities in
302 the Kristianstad Basin ideal for studying sub-annual variability in shell chemistry and reconstructing
303 paleoseasonality and environmental change in the Campanian (Sørensen et al., 2015).

304 **2.2 Bivalve shells**

305 Fossil bivalve shells offer a valuable archive for studying past climates on a seasonal scale. Incremental
306 measurements of shell chemistry in growth direction (sclerochronology studies) potentially yield records of
307 seasonal changes in the environment (Mook, 1971; Jones, 1983; Klein et al., 1996; Schöne and Gillikin,
308 2013). Their distribution allows paleoseasonality reconstructions from bivalves across a wide range of
309 latitudes (Roy et al., 2000; Jablonski et al., 2017), and the preservation potential of calcitic shell structures
310 (especially in oyster shells) makes them ideal, if not unique, recorders of pre-Quaternary seasonality and
311 sub-annual environmental change (Brand and Veizer, 1980; 1981; Al-Aasm and Veizer, 1986a; b;
312 Immenhauser et al., 2005; Alberti et al., 2017). The incremental deposition of shell carbonate means, in
313 theory, that the limits in terms of time resolution of the bivalve shell archive are governed by sampling
314 resolution rather than the resolution of the record itself. While periods of growth cessation can occur
315 (especially in high latitudes, Ullmann et al., 2010) and the true mechanisms of shell deposition on a very
316 high (e.g. daily) temporal resolution are poorly constrained (see de Winter et al., 2020a and references
317 therein), in practice incremental shell deposition allows reconstructions of changes down to sub-daily
318 timescales given the right sampling techniques (Schöne et al., 2005; Sano et al., 2012; Warter et al., 2018;
319 de Winter et al., 2020a). Examples of chemical proxies used in such sclerochronology studies include stable
320 carbon and oxygen isotope ratios and trace element ratios (e.g. Steuber et al., 2005; Gillikin et al., 2006;
321 McConnaughey and Gillikin, 2008; Schöne et al., 2011; de Winter et al., 2017a; 2018).

322 **2.3 Trace element proxies**

323 The incorporation of trace elements and carbon isotopes into bivalve shells is influenced by so-called vital
324 effects: biological controls on the incorporation of elements in the shell independent of the environment
325 (Weiner and Dove, 2003; Gillikin et al., 2005). These vital effects have been shown to mask the
326 characteristic relationships between shell trace element chemistry and the environment and appear to be
327 distinct not only between different bivalve species but also between specimens of different ontogenetic age
328 (Freitas et al., 2008). Differences between bivalve families mean that the trace element chemistry of some
329 taxa (like scallops: Family Pectinidae) are especially affected by vital effects (Lorrain et al., 2005; Freitas
330 et al., 2008), while other families like oysters (Family Ostreidae) seem to be more robust recorders of
331 environmental conditions (Surge et al., 2001; Surge and Lohmann, 2008; Ullmann et al., 2010; 2013). The
332 effect on shell composition and preservation of changes in microstructure and the amount of organic matrix

333 present in different shell layers introduces uncertainty as to which parts of the shells are well-suited for
334 reconstruction purposes (Carriker et al., 1991; Kawaguchi et al., 1993; Dalbeck et al., 2006; Schöne et al.,
335 2010; 2013). The key to disentangling ~~these~~ vital effects from recorded environmental changes lies in the
336 application of multiple proxies and techniques on the same bivalve shells (the “multi-proxy approach”; e.g.
337 Ullmann et al., 2013; de Winter et al., 2017a; 2018) and to base reconstructions on more than one shell
338 (Ivany, 2012).

339 **2.4 Stable isotope ratios**

340 Because nearly all bivalves precipitate their shells at or near oxygen isotope equilibrium, the stable oxygen
341 isotope ratio of bivalve shell carbonate is less susceptible to vital effects, such as growth kinetics (Uchikawa
342 and Zeebe, 2012). Therefore, stable oxygen isotope ratios in bivalve shell carbonate ($\delta^{18}\text{O}_c$) are solely
343 dependent on calcification temperature and sea water oxygen isotope composition ($\delta^{18}\text{O}_{sw}$), and this proxy
344 is frequently used in sclerochronology studies as a paleothermometer (Kim and O'Neil, 1997; Schöne et
345 al., 2005; Butler et al., 2013; Ullmann et al., 2013; Huyghe et al., 2015; de Winter et al., 2020b). Oxygen
346 isotope records can function as a reference in the above-mentioned multi-proxy studies aimed at resolving
347 vital effects, environmental and climatic changes. However, the weakness of this proxy lies in the fact that
348 $\delta^{18}\text{O}_{sw}$ is not always known, especially in deep time settings (Veizer and Prokoph, 2015). As a result, a
349 constant $\delta^{18}\text{O}_{sw}$ of 0‰VSMOW for modern icehouse climate conditions, or -1‰VSMOW for an ice-free
350 world (such as the Eocene or the Late Cretaceous; after Shackleton, 1986) is often assumed (e.g.
351 Andreasson and Schmitz, 1996; Ivany and Runnegar, 2010; Huyghe et al., 2015). An offset of 1‰ between
352 assumed $\delta^{18}\text{O}_{sw}$ and actual $\delta^{18}\text{O}_{sw}$ can result in a ~4.6°C temperature offset in temperature reconstructions
353 (Kim and O'Neil, 1997) This assumption may therefore introduce inaccuracies in absolute temperature
354 reconstructions, but relative variations in $\delta^{18}\text{O}_c$ can still yield important insights into high-resolution climate
355 dynamics.

356 In marine mollusks, dissolved inorganic carbon (DIC) in the ambient sea water contributes the largest
357 fraction of carbon (90%) used for shell mineralization (McConnaughey, 2003; Gillikin et al., 2007) and
358 therefore heavily influences $\delta^{13}\text{C}$ values of shell carbonate. However, changes in respiration rates can alter
359 the carbon budget of shell carbonate by adding or removing isotopically light respired carbon in the form of

360 CO₂ (Lorrain et al., 2004). Environmental changes in DIC can also have a strong influence on this carbon
361 budget, especially when bivalves grow in nearshore or estuarine conditions with large (seasonal) variations
362 in environmental $\delta^{13}\text{C}$ of DIC and organic carbon (Gillikin et al., 2006). Conceptual models exist that attempt
363 to correlate shell $\delta^{13}\text{C}$ in modern mollusks to environmental and physiological variations, but these require
364 knowledge of ambient CO₂ pressures and $\delta^{13}\text{C}$ values of DIC, gas ventilation rates in the animal and CO₂
365 and O₂ permeabilities of calcifying membranes (McConnaughey et al., 1997), which are not available in
366 fossil bivalve studies.

367 **2.5 Aim**

368 In this study, we present a detailed, multi-proxy comparison of the growth and chemistry of well-preserved
369 fossil shells of the thick-shelled oyster *Rastellum diluvianum* (Linnaeus, 1767) recovered from the Ivö Klack
370 locality on the northern edge of the Kristianstad Basin. We combine stable isotope proxies conventional in
371 sclerochronological studies ($\delta^{13}\text{C}$ and $\delta^{18}\text{O}$; e.g. Goodwin et al., 2001; Steuber et al., 2005) with less well-
372 established trace element proxies (Mg/Ca, Sr/Ca, Mg/Li and Sr/Li; e.g. Bryan and Marchitto, 2008; Schöne
373 et al., 2011; Füllenbach et al., 2015; Dellinger et al., 2018) and growth modelling based on $\delta^{18}\text{O}$ seasonality
374 (Judd et al., 2018) in an attempt to disentangle the effects of growth rate, reproductive cycle and
375 environmental change on shell chemistry. The data gathered in this study allow a detailed discussion on
376 seasonal changes in temperature and water chemistry in the coastal waters of the Kristianstad Basin in the
377 late early Campanian, as well as on the life cycle of *R. diluvianum* and its response to seasonal changes in
378 its environment.

379

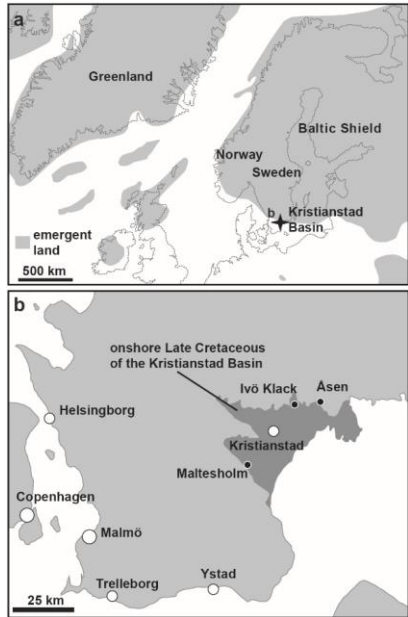


Figure 1: Paleogeographic map of the Boreal Chalk Sea (a) and the area of present-day southern Sweden (b) showing the location of Ivö klack (modified after Sørensen et al., 2015)

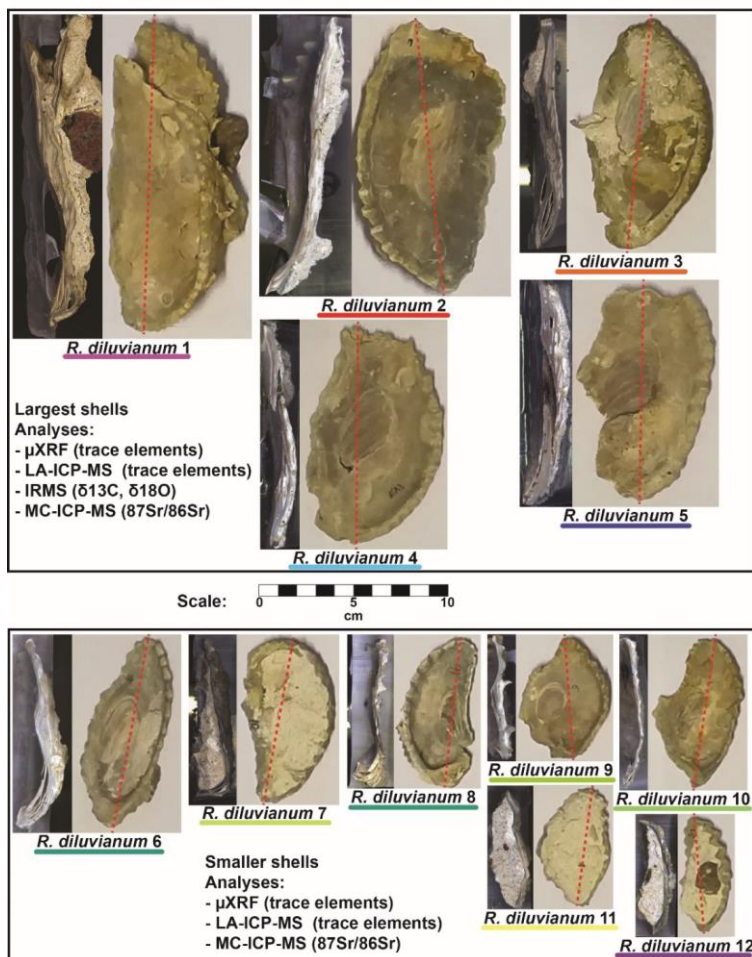
382 **3. Materials and Methods**

383 **3.1 Sample acquisition and preparation**

384 Complete valves of twelve individual *R. diluvianum* oysters were obtained from the Ivö Klack locality (see
385 **Fig. 2**). Specimens of *R. diluvianum* were found *in situ* attached to the vertical sides of large boulders that
386 characterized the rocky shore of Ivö Klack (Surlyk and Christensen, 1974) and are biostratigraphically
387 assigned to the latest early Campanian *B. mammillatus* belemnite zone. The valves were cleaned and fully
388 embedded in Araldite® 2020 epoxy resin (Bodo Möller Chemie Benelux, Antwerp, Belgium). Dorsoventral
389 slabs (± 10 mm thick) were cut perpendicular to the hinge line using a water-cooled slow rotating saw with
390 a diamond-coated blade (thickness ± 1 mm; **Fig. 2**). The surfaces cut on the central growth axis were
391 progressively polished using silicon-carbide polishing disks (up to P2500, or 8.4 μm grain size). Polished
392 surfaces were scanned at high (6400 dpi) resolution using an Epson Perfection 1650 flatbed color scanner
393 (Seiko Epson Corp., Suwa, Japan). Resulting color scans of all polished *R. diluvianum* shell cross sections
394 are provided in **Fig. 2** and **S1**. Shell microstructures in *R. diluvianum* shells were studied in detail on high-
395 resolution scans and by using reflected light optical microscopy. Microstructural features were used to
396 reconstruct the relative timing of shell growth (see **Fig. 3**). Fragments of visually well-preserved material
397 from different microstructures in the shells were coated with gold and studied under a Scanning Electron
398 Microscope (Quanta 200 ESEM) and imaged at 1000x – 2000x magnification (**Fig. 3b-e**). Chemical
399 analyses were carried out sequentially on polished cross sections in order of destructive character of
400 sampling (starting with the least destructive measurements: μXRF , LA-ICP-MS, microdrilling for IRMS and
401 finally MC-ICP-MS analysis on ~ 26 mg samples).

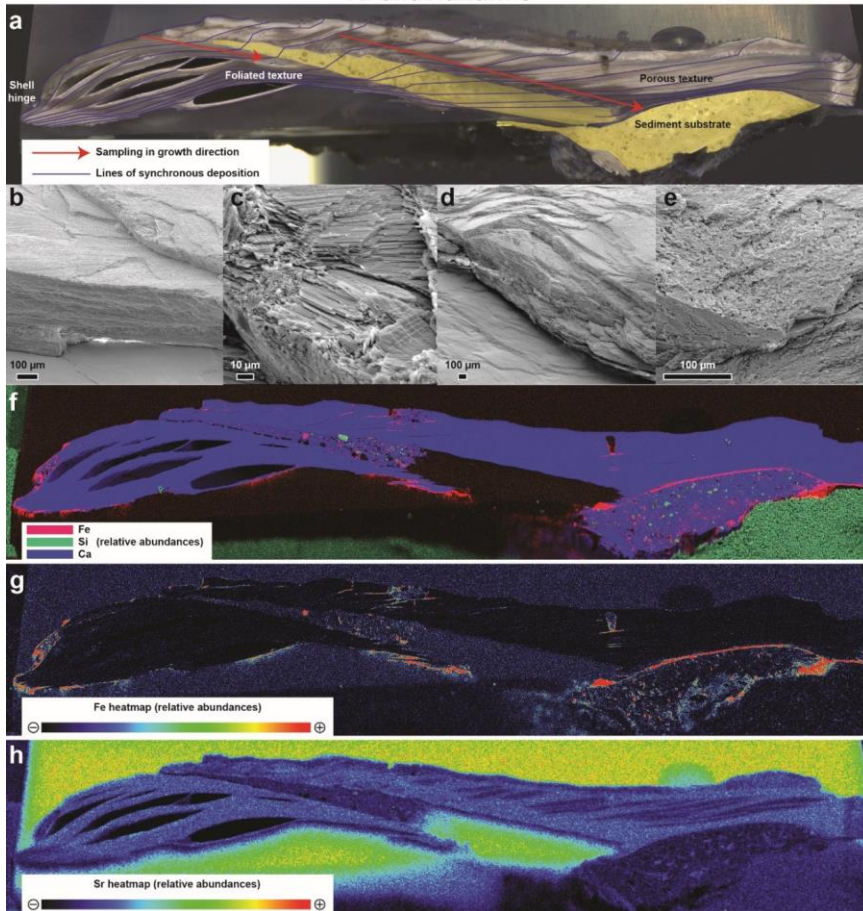
402

Overview of *Rastellum diluvianum* shells



403 **Figure 2:** Overview of the 12 *Rastellum diluvianum* shells used in this study. All shells are depicted ~~on~~ at the same scale (see scalebar
 404 in center of image). Colors of the lines under sample names correspond to the colors of the lines in Fig. 4, Fig. 6, Fig. 8 and Fig. 10.
 405 Every shell is represented by an image of the inside of the valve analyzed, as well as a color scan of the cross section through the
 406 shell on which high-resolution analyses were carried out. Dashed red lines show the location of these cross sections. The largest 5
 407 shells (1-5, on top half) were sampled for IRMS analyses ($\delta^{13}\text{C}$ and $\delta^{18}\text{O}$). All shells were subjected to micro X-ray fluorescence
 408 (μXRF), laser ablation inductively coupled plasma mass spectrometry (LA-ICP-MS) and multi-cup inductively coupled plasma mass
 409 spectrometry (MC-ICP-MS) analyses. Full-size versions of the high-resolution color scans of shell cross sections are provided in **S1**.
 410

R. diluvianum 3



411
412 **Figure 3:** Overview image showing a high-resolution color scan of the cross section through *R. diluvianum* 3 (a) on which the different
413 shell textures as well as the directions of high-resolution analyses (in growth direction) are indicated. Thin blue lines denote parts of
414 the shell that were deposited at the same time (growth increments). Areas marked in yellow represent sediment infilling below and
415 between-within the valves. (b) and (c) show SEM images of the well-preserved foliated calcite in the shell. More porous structures in
416 the shell (vesicular calcite) are depicted in SEM images shown in (d) and (e). Below are shown three XRF elemental maps of the
417 same cross section: An RGB-colored map displaying the relative abundances of Fe, Si and Ca (f), A heatmap of Fe concentrations
418 (g; see scalebar below map) and a heatmap of Sr concentrations (h; see scalebar below map). XRF mapping only yields relative
419 (semi-quantitative) abundance of elements.

420

421 3.2 Micro-XRF mapping

422 Elemental abundance maps of all *R. diluvianum* shell cross sections were obtained using a Bruker Tornado
423 M4 energy-dispersive micro-X-Ray Fluorescence scanner (μ XRF; Bruker nano GmbH, Berlin, Germany).
424 All μ XRF analyses carried out with the Bruker M4 Tornado are non-destructive. The μ XRF is equipped with
425 a Rh filament metal-ceramic tube X-Ray source operated at 50 kV and 600 μ A (30 W; maximum energy
426 settings). The circular spot projected on the same surface is estimated to have a diameter of 25 μ m (Mo-
427 K α). A μ m-precision XYZ translation stage allows for quick and precise sample movement such that a grid
428 of 25 μ m XRF spots can be measured on the sample surface by continuous scanning to construct elemental
429 maps ($3 * 10^6 - 5 * 10^6$ pixels per map). Exposure times of the X-ray beam per sampling position in mapping
430 mode (1 ms/pixel) are too short to gain adequate signal-to-noise ratio for pixel-by-pixel quantification of
431 elemental concentrations. Instead, processing of entire map surfaces using the Bruker Esprit™ software
432 allows semi-quantitative elemental abundance maps to be created of the sample surface based on a
433 mapping of the count rate in 'Regions of Interest' of elements (see de Winter and Claeys, 2016; de Winter
434 et al., 2017b; **Fig. 3**). XRF maps allow for a rapid assessment of the preservation state of original shell
435 calcite based on variations in Si, Mn, Fe and Sr concentrations and guide the selection-formulation of
436 sampling protocols for further analyses (de Winter and Claeys, 2016; **Fig. 3**). Results of XRF mapping on
437 all 12 *R. diluvianum* shell cross sections are provided in **S2**.

438 3.3 Micro-XRF line scans

439 After XRF mapping, quantitative line scans were measured in growth direction on shell cross sections.
440 Dwell times of 60 seconds per measurement yielded sufficiently high signal-to-noise ratios for individual
441 points in line scans to be quantified. This acquisition time was chosen so as to provide the optimal
442 compromise between increasing run time (improved signal/noise ratio; enhanced reproducibility) and
443 increasing the number of sampling positions (improving sampling density and allowing duplicate
444 measurements) for the elements Mg, Al, Si, P, S, Ca, Ti, Mn, Fe, Cu, Zn and Sr (see discussion in de Winter
445 et al., 2017b). The sampling interval of line scans was 50 μ m, adding up to a total of 11056 individual
446 quantitative XRF spectra measured for this study. Spectra were quantified using the Bruker Esprit software
447 calibrated using the matrix-matched BAS-CRM393 limestone standard (Bureau of Analyzed samples,

448 Middlesbrough, UK), after which individual measurements were calibrated offline using 7 matrix-matched
449 certified reference materials (CCH1, COQ1, CRM393, CRM512, CRM513, ECRM782 and SRM1d), which
450 were treated as samples (see Vansteenberge et al., 2020). R^2 values of calibration curves exceeded 0.99
451 and reproducibility standard deviations were better than 10% relative to the mean. Even though line scans
452 were positioned on well-preserved shell calcite based on the XRF map results, a second check was carried
453 out in which individual points were rejected based on conservative thresholds for diagenetic recrystallization
454 or detrital contamination ($[Ca] < 38$ wt%, $[Si] > 1$ wt%, $[Mn] > 200$ $\mu\text{g/g}$ or $[Fe] > 250$ $\mu\text{g/g}$; $[Sr]/[Mn] < 100$
455 mol/mol; see Al-Aasm and Veizer, 1986a; Sørensen et al., 2015). Concentrations of Ca, Mg and Sr in well-
456 preserved shell sections were used to explore the potential of Mg/Ca and Sr/Ca molar ratios as
457 paleoenvironmental proxies. Unprocessed results of XRF line scanning are provided in **S3**.

458 **3.4 LA-ICP-MS line scans**

459 Spatially resolved elemental concentrations for Li, B, Mg, Si, P, Ca, Ti, V, Cr, Mn, Fe, Ni, Zn, Rb, Sr, Ba,
460 Pb and U were calculated from a calibrated transient MS signal recorded during Laser Ablation-Inductively
461 Coupled Plasma-Mass Spectrometry (LA-ICP-MS) line scanning in the growth direction (parallel to the XRF
462 line scans) on shell cross sections. LA-ICP-MS measurements were carried out at the Atomic and Mass
463 Spectrometry – A&MS research unit of Ghent University (Ghent, Belgium) using a 193 nm ArF*excimer-
464 based Analyte G2 laser ablation system (Teledyne Photon Machines, Bozeman, USA), equipped with a
465 HelEx 2 double-volume ablation cell, coupled to an Agilent 7900 quadrupole-based ICP-MS unit (Agilent,
466 Tokyo, Japan). Continuous scanning along shell transects using a laser spot with a diameter of 25 μm ,
467 scan speed of 50 $\mu\text{m/s}$ and detector mass sweep time of 0.5 s yielded profiles with a lateral sampling
468 interval of 25 μm , amounting to a total of 9505 LA-ICP-MS data points gathered. The aerosol was
469 transported using He carrier gas into the ICP-MS unit via the aerosol rapid introduction system (ARIS;
470 Teledyne Photon Machines, Bozeman, USA). Elemental concentrations were calibrated using bracketed
471 analysis runs on US Geological Survey (USGS) BCR-2G, BHVO-2G, BIR-1G, GSD-1G and GSE-1G and
472 National Institute of Standards and Technology (NIST) SRM612 and SRM610 certified reference materials.
473 Calcium concentrations (measured via ^{43}Ca) were used as internal standard for data normalization and drift
474 correction during the measurement campaign, and Ca concentrations of 38.5 wt% were assumed for
475 pristine shell carbonate. Coefficients of determination (R^2) of a linear model fitted to the calibration curves

476 were better than 0.99 and the standard deviation of reproducibility for elemental concentrations was better
477 than 5% relative to the mean value. Individual LA-ICP-MS measurements were inspected for diagenetic
478 alteration or contamination by detrital material using the same thresholds as used for XRF data (see above).
479 LA-ICP-MS and μ XRF measurements were combined to cover a wider range of elements, since some
480 elements (e.g. S and Sr) were measured more reliably using μ XRF, while others (e.g. Li or Ba) could only
481 be quantified using LA-ICP-MS. Concentrations of Li, Mg, and Sr were used to explore the potential of
482 Mg/Li and Sr/Li molar ratios as proxies for paleoenvironmental change. Unprocessed results of LA-ICP-MS
483 line scans are provided in **S4**.

484 **3.5 Isotope Ratio Mass Spectrometry**

485 A transect of powdered samples (± 200 μ g) was ~~sampled~~extracted for Isotope Ratio Mass Spectrometry
486 (IRMS) analysis in growth direction along well-preserved foliated calcite (**Fig. 3**) in the five largest of the
487 twelve *R. diluvianum* shells (*R. diluvianum* 1-5; see **Fig. 2**) using a microdrill (Merchantek/Electro Scientific
488 Industries Inc., Portland (OR), USA) equipped with a 300 μ m diameter tungsten carbide drill bit, coupled to
489 a microscope (Leica GZ6, Leica Microsystems GmbH, Wetzlar, Germany). A total of 531 IRMS samples
490 were taken at an interspacing of 250 μ m. Stable carbon and oxygen isotope ratios ($\delta^{13}\text{C}$ and $\delta^{18}\text{O}$) were
491 measured in a NuPerspective IRMS equipped with a NuCarb carbonate preparation device (Nu
492 Instruments, UK). The sample size (50-100 μ g) allowed duplicate measurements to be carried out regularly
493 (roughly once every 30 samples) to assess reproducibility. Samples were digested in 104% phosphoric
494 acid at a constant temperature of 70°C and the resulting CO_2 gas was cryogenically purified before being
495 led into the IRMS through a dual inlet system. Isotope ratios were corrected for instrumental drift and
496 fractionation due to variations in sample size and the resulting values are reported relative to the Vienna
497 Pee Dee Belemnite standard (‰VPDB) using repeated measurements of the IA-603 stable isotope
498 standard (International Atomic Energy Agency, Vienna, Austria). Reproducibility of $\delta^{18}\text{O}$ and $\delta^{13}\text{C}$
499 measurements on this standard were better than 0.1‰ and 0.05‰ (1σ ; N=125) respectively. All stable
500 isotope analysis results are provided in **S5** and plots of stable isotope and trace element records from all
501 shells are given in **S6**.

502 **3.6 Growth and age modelling**

503 Stable oxygen isotope curves measured in *R. diluvianum* were used to produce age models for the growth
504 of the shell using a bivalve growth model written in MatLab (Mathworks, Natick, MA, USA) which simulates
505 $\delta^{18}\text{O}$ curves using a combination of growth and temperature sinusoids (Judd et al., 2018). This simulation
506 model was modified to calculate its temperatures based on calcite $\delta^{18}\text{O}$ (following Kim and O'Neil, 1997)
507 rather than from the aragonite $\delta^{18}\text{O}$ -temperature relationship used in the original approach (after Grossman
508 and Ku, 1986; see Judd et al., 2018). A value of -1.0‰ VSMOW was assumed for $\delta^{18}\text{O}$ of Campanian
509 ocean water (Shackleton, 1986; Thibault et al., 2016). Additional minor modifications in the source code
510 allowed results of intermediate calculation steps in the model to be exported. The modified Matlab source
511 code is provided in **S7**. Note that this model assumes that the shape and absolute value of $\delta^{18}\text{O}$ curves
512 depend solely on water temperature and growth rate (ignoring changes in $\delta^{18}\text{O}_{\text{sw}}$), and that a modelled year
513 contains 365 days by construction (while this number should be slightly larger in the Late Cretaceous; de
514 Winter et al., 2020a). Despite these caveats, shell chronologies reconstructed from seasonal patterns in
515 $\delta^{18}\text{O}$ should still be reliable as they are only based on the shape of the $\delta^{18}\text{O}$ curves. Uncertainties on
516 modelled temperature curves were derived by propagating the measurement uncertainty on $\delta^{18}\text{O}$. Age
517 models thus obtained for shells *R. diluvianum* 1-5 were used to align all proxy records on a common time
518 axis. Age models for *R. diluvianum* 6-12 were constructed by extrapolating relationships between modelled
519 seasonality and microstructures and trace element concentrations observed in *R. diluvianum* 1-5.
520 Simultaneously deposited microstructural features in shell cross sections (see **Fig. 3**) were used to
521 determine the actual dorsoventral height of the shells at different ages, linking shell height to the age and
522 allowing the construction of growth curves for all twelve *R. diluvianum* shells. The total age and the season
523 of spawning (or: the start of shell growth) were determined by extrapolating the $\delta^{18}\text{O}$ -based age models
524 and by using the relationship between $\delta^{18}\text{O}$ profiles and trace element records and growth increments
525 observed in the shell.

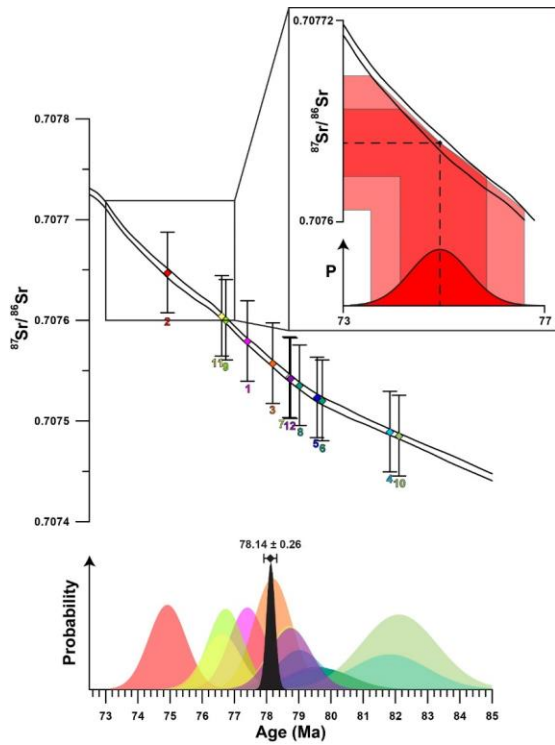
526 **3.7 Strontium isotope analysis**

527 Samples (on average 26 mg) for strontium isotope analysis were obtained by drilling the well-preserved
528 foliated calcite in all shells using a Dremel 3000 dental drill with a 0.5 mm tungsten carbide drill bit. Calcite
529 samples were placed in Teflon beakers (Savillex LLC, Eden Prairie, MN, USA), dissolved in subboiled

530 concentrated (14 M) nitric acid (HNO₃) at 120°C and left to dry out at 90°C overnight, after which the residue
531 was redissolved in 2 M HNO₃. Carbonate-bound strontium in the samples was purified following the ion-
532 exchange resin chromatography method detailed in Snoeck et al. (2015). The ⁸⁷Sr/⁸⁶Sr of purified Sr
533 samples were determined using a Nu Plasma (Nu Instruments Ltd, Wrexham, UK) multi-collector (MC) ICP-
534 MS unit in operation at the Université Libre de Bruxelles (ULB). During the measurement run, repeated
535 analyses of NIST SRM987 standard solution yielded a ratio of 0.710250 ± 0.000040 (2 SD; N = 14),
536 statistically consistent with the literature value of 0.710248 ± 0.000058 (2 s.e.; McArthur et al., 2001; Weis
537 et al., 2006). All results were corrected for instrumental mass discrimination by internal normalization and
538 normalized to the literature value of NIST SRM987 (0.710248) through a standard-sample bracketing
539 method. For each sample, ⁸⁷Sr/⁸⁶Sr are reported with 2σ uncertainty (**S8**).

540

541



542 **Figure 4:** Plot showing the results of Sr-isotopic analyses with error bars (2σ) plotted on the Sr-isotope curve of
543 McArthur et al. (2016; top of image). Numbers below the error bars indicate specimen number. Measurements from the
544 12 specimens of *R. diluvianum* are represented by parallelograms in different colors which match the probability
545 distributions plotted below. The probability distribution curves in the lower pane show the distribution of uncertainty on
546 each Sr-isotope measurement as well as the uncertainty on the Sr-isotope curve propagated to the age domain (colors
547 of individual shells are the same as in Fig. 2). Insert shows schematically how uncertainties of the isotope
548 measurements as well as the isotope curve are propagated into the age domain. The black curve shows the total
549 uncertainty distribution function compiled from the 12 individual measurements following Barlow (2004), with the
550 combined age estimate including uncertainty (2σ) shown above.

551

552

553 3.8 Strontium isotope dating

554 *R. diluvianum* specimens were independently dated by comparing $^{87}\text{Sr}/^{86}\text{Sr}$ values measured in the
555 samples with the Sr-isotope curve in the 2016 Geological Timescale (McArthur et al., 2016). Uncertainties
556 in $^{87}\text{Sr}/^{86}\text{Sr}$ measurements were propagated into dates by finding the closest date of the mean $^{87}\text{Sr}/^{86}\text{Sr}$
557 value as well as the dates of the minimum (-2σ) and maximum ($+2\sigma$) $^{87}\text{Sr}/^{86}\text{Sr}$ values by linearly interpolating
558 ages in the $^{87}\text{Sr}/^{86}\text{Sr}$ curve matching the measured $^{87}\text{Sr}/^{86}\text{Sr}$ value, including the uncertainty estimated on
559 the Sr-isotope curve itself. A composite age for the Ivö Klack deposits was obtained by combining the age
560 uncertainty distributions of the individually dated $^{87}\text{Sr}/^{86}\text{Sr}$ samples into a single age. Due to the non-linear
561 shape of the $^{87}\text{Sr}/^{86}\text{Sr}$ curve, uncertainties on the $^{87}\text{Sr}/^{86}\text{Sr}$ ages were asymmetrical. Since no mathematical
562 solution exists for the combination of asymmetric uncertainties, the asymmetric uncertainty on the total age
563 had to be approximated through maximum likelihood estimation using the combined log likelihood function
564 (Barlow, 2003). The approximation of the total uncertainty of combined $^{87}\text{Sr}/^{86}\text{Sr}$ dating results in this study
565 was carried out using the mathematical approach of Barlow (2004) in R (R Core Team, 2013; Roger Barlow,
566 personal communication; code available on <https://zenodo.org/record/1494909>). The uncertainty interval of
567 the composite age is represented by 2 times the standard error (~95.5% confidence level). A plot of the
568 uncertainty distributions of the individual specimens and the total uncertainty distribution is shown in **Fig.**
569 **4**. Raw $^{87}\text{Sr}/^{86}\text{Sr}$ data are provided in **S8**.

570

571 4. Results

572 4.1 Strontium isotope dating

573 Results of strontium isotope analyses are given in **S8**. The mean strontium isotope ratio of all *R. diluvianum*
574 specimens is 0.707552 (± 0.000112 ; 95% confidence level). The compilation of $^{87}\text{Sr}/^{86}\text{Sr}$ results from 12
575 specimens of *R. diluvianum* (**Fig. 4**) shows how age estimates from individual specimens have considerable
576 uncertainties (standard deviations around 1 Myr, see **S8**), yet the uncertainty on the composite age is
577 significantly smaller. The composite age for the Ivö Klack deposits is 78.14 Ma (± 0.26 ; 95% confidence

578 level). This result places the age of the Ivö Klack deposits close to the early/late Campanian boundary when
579 applying a twofold division of the Campanian and in the middle Campanian when applying a threefold
580 division scheme (Ogg et al., 2016). This age estimate is similar to the age obtained when plotting the *B.*
581 *mammilatus* zone on the recent integration schemes of the Campanian (Wendler, 2013). Earlier estimates
582 (Christensen, 1997; Surlyk and Sørensen, 2010; Sørensen et al., 2015) yielded ages about 2-4 Myr older
583 (80-82 Ma), but those relied on presently outdated and partly incorrect age models.

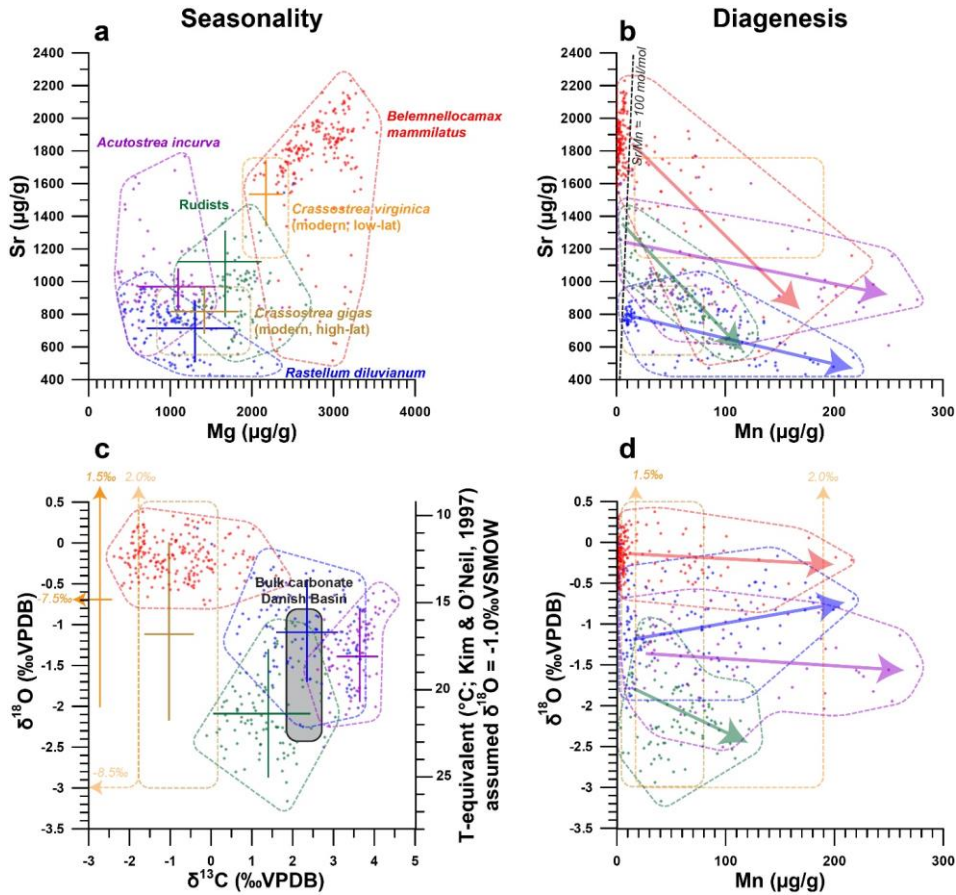
584 **4.2 Shell structure and preservation**

585 A combination of high-resolution color scans, SEM images and μ XRF mapping of shell cross sections
586 reveals that *R. diluvianum* shells consist of thin layers of dark, foliated calcite, interwoven with lighter, more
587 porous carbonate layers (**Fig. 3a-e**). The latter are characterized by higher concentrations of Mn, Fe and
588 Si and lower Sr concentrations (**Fig. 3f-h**). Foliated calcite layers are more densely packed on the inside of
589 the shell, especially in the region of the adductor muscle scar, and at the shell hinge (**Fig. 3a**). They are
590 characterized by high Sr concentrations and low concentrations of Mn, Fe and Si (**Fig. 3f-h; S2**). Further
591 away from the shell hinge and the inside of the valve, porous carbonate layers become more dominant. In
592 these regions, μ XRF mapping also clearly shows that detrital material (high in Si and Fe) is often found
593 between the shell layers (**Fig. 3f**). SEM images show that the shell structure of *R. diluvianum* strongly
594 resembles that of modern oyster species, as described in previous studies (**Fig. 3b-e**; Carriker et al., 1979;
595 Surge et al., 2001; Ullmann et al., 2010; 2013; Zimmit et al., 2018). The major part of the shell consists of
596 calcite, of which the foliated structures were sampled for chemical analyses in this study. As in modern
597 oyster species, aragonite may originally have been deposited on the resilium of the shell, but this region is
598 not considered for analyses (see outer tip of shell hinge in **Fig. 3a**; Stenzel, 1963; Carriker et al., 1979;
599 Sørensen et al., 2012). Close similarities with modern oysters allow to infer that shell growth in *R.*
600 *diluvianum* occurred in a similar way ~~as it does in~~to modern oyster species like *Ostrea edulis*, *Crassostrea*
601 *virginica* and *C. gigas*. ~~From this extrapolation~~On this basis we could estimate the total shell height at
602 specific times in ontogeny from microstructural growth markers (dashed lines in **Fig. 3a**; following Zimmit et
603 al., 2018), linking growth to changes in shell chemistry.

604 **4.3 Trace element analyses results**

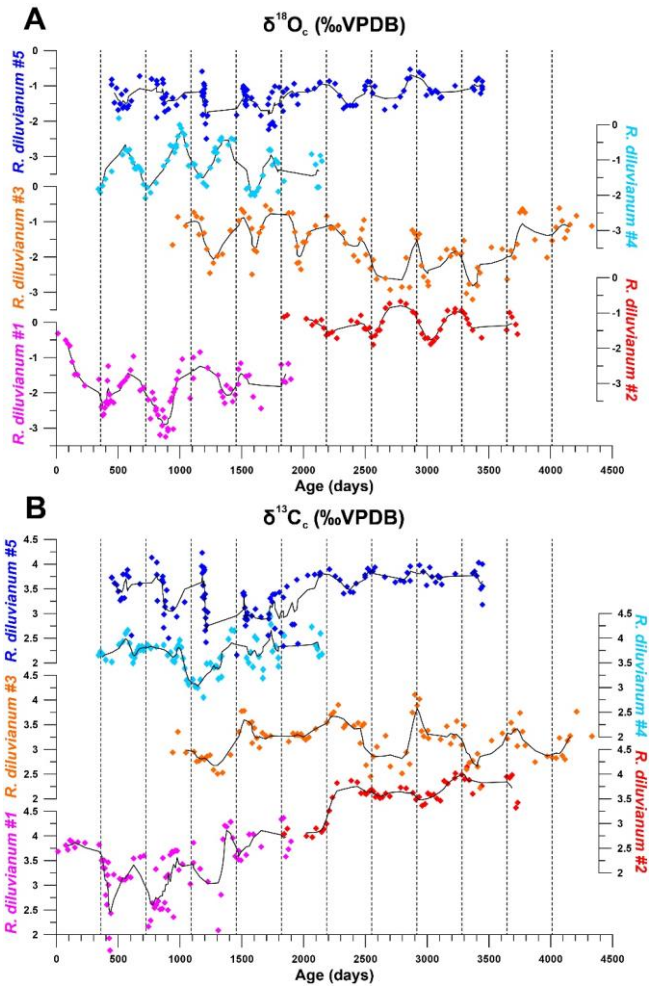
605 The similarity in growth between *R. diluvianum* and modern oyster species is used to assess whether trace
606 element variability in *R. diluvianum* can be interpreted in terms of environmental changes in a similar way
607 as in modern oyster shells (e.g. Surge and Lohmann, 2008; Ullmann et al., 2013; Mouchi et al., 2013;
608 Dellinger et al., 2018). The combination of μ XRF and LA-ICP-MS analyses on *R. diluvianum* shells resulted
609 in records of changes in Mg/Ca, Sr/Ca (μ XRF), Mg/Li and Sr/Li (LA-ICP-MS) as well as individual
610 concentrations of trace elements such as Mg, Mn, Fe and Sr (**Figure 5**). All chemical analyses were carried
611 out on the dense foliated calcite exposed in cross sections close to the inner edge of the shell valve (**Fig.**
612 **3a**). High-resolution color scans and detailed recording of sampling positions allowed these records to be
613 plotted on a common axis (see **S6, S10**). In **Fig. 5**, results of chemical analyses of *R. diluvianum* specimens
614 (including diagenetically altered parts) are compared with data from three other mollusk taxa (the belemnite
615 *Belemnelloccamax mammillatus*, the oyster *Acutostrea incurva* and the radiolithid rudist *Biradiolites*
616 *suecicus*) from Ivö Klack (Sørensen et al., 2015), as well as data from extant oysters (Rucker and Valentine,
617 1961; Surge et al., 2001; Ullmann et al., 2013). Multi-proxy analysis revealed periodic variations in stable
618 isotope and trace element ratios (see **Fig. 6**). The amplitudes of these variations plotted in **Fig. 5** show that
619 Mg and Sr concentrations measured in all three fossil bivalve taxa are similar, while concentrations in the
620 belemnite rostra are much higher. Finally, plots in **Fig. 5b** and **Fig. 5d** demonstrate that diagenetic alteration
621 (evident from elevated Mn concentrations) reduces the Sr concentration in carbonate of all four taxa. Stable
622 oxygen isotope ratios of the shells are affected to a lesser degree (see below). The majority of
623 measurements in all four taxa show very little signs of diagenetic alteration, with most measurements
624 characterized by low (< 100 μ g/g) Mn concentrations (**Fig. 5**).

625



626

627 **Figure 5:** Cross plots summarizing the results of trace element and stable isotope analyses of the oysters *R. diluvianum* (blue), *A.*
 628 *incurva* (purple), the rudist *Biradiolites suecicus* (green) and the belemnite *B. mammilatus* (red, after Sørensen et al., 2015) from the
 629 Kristianstad basin. Results from modern *C. gigas* (brown; Ullmann et al., 2013) and *C. virginica* (yellow; Rucker and Valentine, 1961;
 630 Surge et al., 2001) oysters are plotted for comparison. Points indicate individual data points, drawn polygons illustrate the range of
 631 the data and crosses indicate the extent of seasonality (if present). (a) Strontium concentrations plotted against magnesium
 632 concentrations. (b) Strontium concentrations plotted against manganese concentrations. Arrows indicate the interpreted direction of
 633 diagenetic alteration and the black dashed line shows the Sr/Mn diagenesis threshold proposed for belemnite rostra by Sørensen et
 634 al. (2015; 100 mol/mol). (c) $\delta^{18}\text{O}$ plotted against $\delta^{13}\text{C}$. Grey area indicates the range of stable isotope ratios measured in Campanian
 635 chalk deposits from the nearby Danish Basin by Thibault et al. (2016) (d) $\delta^{18}\text{O}$ plotted against manganese concentrations, with arrows
 636 indicating proposed direction of diagenetic alteration.



638
 639 **Figure 6:** Overview of stable oxygen (A) and carbon (B) profiles from all five shells in which stable isotope profiles are/were measured
 640 plotted against ontogenetic ages. Black lines indicate 5-point running averages through the time series. Vertical dashed lines separate
 641 years of growth. All vertical axes of $\delta^{18}\text{O}$ and $\delta^{13}\text{C}$ have the same scale. Colors coding is the same as in **Figure 7**.

642

643 4.4 Stable isotope records

644 An overview of stable isotope results of *R. diluvianum* (IRMS, only for shells 1-5, see **Fig. 2**) compared with
645 the different taxa in Kristianstad Basin and modern oyster data is given in **Figure 5**. Stable isotope ratios
646 of the rudist and oyster shells overlap, while belemnite rostra of the species *B. mammillatus* are
647 characterized by much lower $\delta^{13}\text{C}$ and ~~heavier~~ higher $\delta^{18}\text{O}$ values. This suggests that $\delta^{13}\text{C}$ in belemnite
648 rostra from this species are affected by vital effects while heavier $\delta^{18}\text{O}$ values of the belemnites suggest
649 that belemnites lived most of their life away from the coastal environment (in deeper waters), as previously
650 suggested by Sørensen et al. (2015). In contrast, stable isotope ratios recorded in the bivalve shells overlap
651 and match the isotope ratios measured in Campanian chalk deposited in the neighboring Danish Basin
652 (Thibault et al., 2016). Records of $\delta^{13}\text{C}$ and $\delta^{18}\text{O}$ in the growth direction through *R. diluvianum* shells exhibit
653 periodic variations (**Figure 6**). These variations are much more regular in $\delta^{18}\text{O}$ records, which show extreme
654 values below -3‰ and up to 0‰ VPDB (**Fig. 6a**). Some shells, such as *R. diluvianum* 3 (**Fig. 7**), exhibit
655 longer term trends on which these periodic variations are superimposed. These trends suggest the
656 presence of multi-annual cyclicity with a period in the order of 10-20 years, but the length of *R. diluvianum*
657 records (max. 10 years) is smaller than the estimated period of these changes and is therefore insufficient
658 to statistically validate the presence of this cyclicity.

659 The extreme values in $\delta^{18}\text{O}$ records translate to tentative temperatures in the range of extremes of 12°C to
660 26°C when assuming a constant $\delta^{18}\text{O}_{\text{sw}}$ value of -1.0‰ (e.g. Thibault et al., 2016) and applying the
661 temperature relationship of Kim and O'Neil (1997). However, the assumption of constant $\delta^{18}\text{O}_{\text{sw}}$ may add
662 bias to the temperature reconstructions, as seawater composition may not have been constant or reflect
663 the marine value year-round in the nearshore Ivö Klack setting. Carbon isotope ratios ($\delta^{13}\text{C}$) do not always
664 follow the same trends as $\delta^{18}\text{O}$ records (**Fig. 6b**). In many parts of *R. diluvianum* shells, there is a clear
665 covariation between the two isotope ratios, suggesting $\delta^{13}\text{C}$ is affected by seasonal changes. However, in
666 other parts this correlation is less clear, suggesting that other (non-seasonal) factors play a role in
667 determining the $\delta^{13}\text{C}$ of shell material.

668 4.5 Age models

669 Modelling the growth of *R. diluvianum* bivalves from seasonal variations in $\delta^{18}\text{O}$ profiles yielded age models,
670 growth rate estimates and reconstructions of water temperature variations during the lifetime of the bivalves.
671 Due to the clear seasonal patterns in $\delta^{18}\text{O}$ records (**Fig. 6a**, **Fig. 7**), modelled $\delta^{18}\text{O}$ profiles closely
672 approximated the measured $\delta^{18}\text{O}$ profiles (total $R^2 = 0.86$, $N = 412$, see **S5** and **S9**), lending high confidence
673 to shell age models (see example in **Fig. 7**). Modelling allowed all proxies measured in the shells of *R.*
674 *diluvianum* to be plotted against shell age, clearly revealing the influence of seasonal variations in
675 environmental parameters on shell chemistry (**S10**). The age models reveal clear, statistically significant (p
676 < 0.05) ontogenetic trends in Mg/Li, Sr/Li and $\delta^{13}\text{C}$ in nearly all specimens of *R. diluvianum* (see **Table 1**).
677 In 3 out of 5 shells, $\delta^{13}\text{C}$ increases with age (see **Fig. 6b** and **Table 1**) with ontogenetically older specimens
678 (e.g. *R. diluvianum* #2) yielding overall higher $\delta^{13}\text{C}$ values (**Fig. 6b**). The distribution of slopes of ontogenetic
679 trends in Li/Ca cannot be distinguished from random variation. Therefore, no ~~predictable-widely-shared~~
680 ontogenetic trends were found for Li-proxies in *R. diluvianum* shells.

681

	Li/Ca			$\delta^{13}\text{C}$		
	slope (mol/(mol*yr))	R2	p-value	slope (‰/yr)	R2	p-value
<i>R. diluvianum 1</i>	-1.29E-06	0.053	4.32E-08	0.346	0.426	8.86E-07
<i>R. diluvianum 2</i>	3.74E-07	0.101	2.68E-05	0.169	0.440	8.19E-08
<i>R. diluvianum 3</i>	3.86E-07	0.004	5.32E-03	-0.004	0.001	8.09E-01
<i>R. diluvianum 4</i>	-1.07E-06	0.025	8.78E-04	0.023	0.009	3.99E-01
<i>R. diluvianum 5</i>	-1.94E-06	0.030	6.30E-14	0.136	0.492	5.53E-11
<i>R. diluvianum 6</i>	-2.32E-06	0.117	8.75E-15			
<i>R. diluvianum 7</i>	-7.49E-07	0.029	4.77E-02			
<i>R. diluvianum 8</i>	-1.19E-07	0.003	2.90E-01			
<i>R. diluvianum 9</i>	-4.63E-07	0.010	5.65E-02			
<i>R. diluvianum 10</i>	1.59E-06	0.015	1.61E-02			
<i>R. diluvianum 11</i>	-1.87E-06	0.199	4.25E-12			
<i>R. diluvianum 12</i>	-4.55E-07	0.003	4.19E-01			
	$p(\chi^2)$		0.976	$p(\chi^2)$		1.000
	$p(\chi^2)$ weighed by R2		0.976	$p(\chi^2)$ weighed by R2		1.000
	$p(\chi^2)$ weighed by p-value		0.961	$p(\chi^2)$ weighed by p-value		0.998

682

683 **Table 1:** Overview of the slopes of ontogenetic trends in Li/Ca and $\delta^{13}\text{C}$ records. P-values on the bottom of the table show that the
684 distribution of Li/Ca slopes is statistically indistinguishable from random.

685

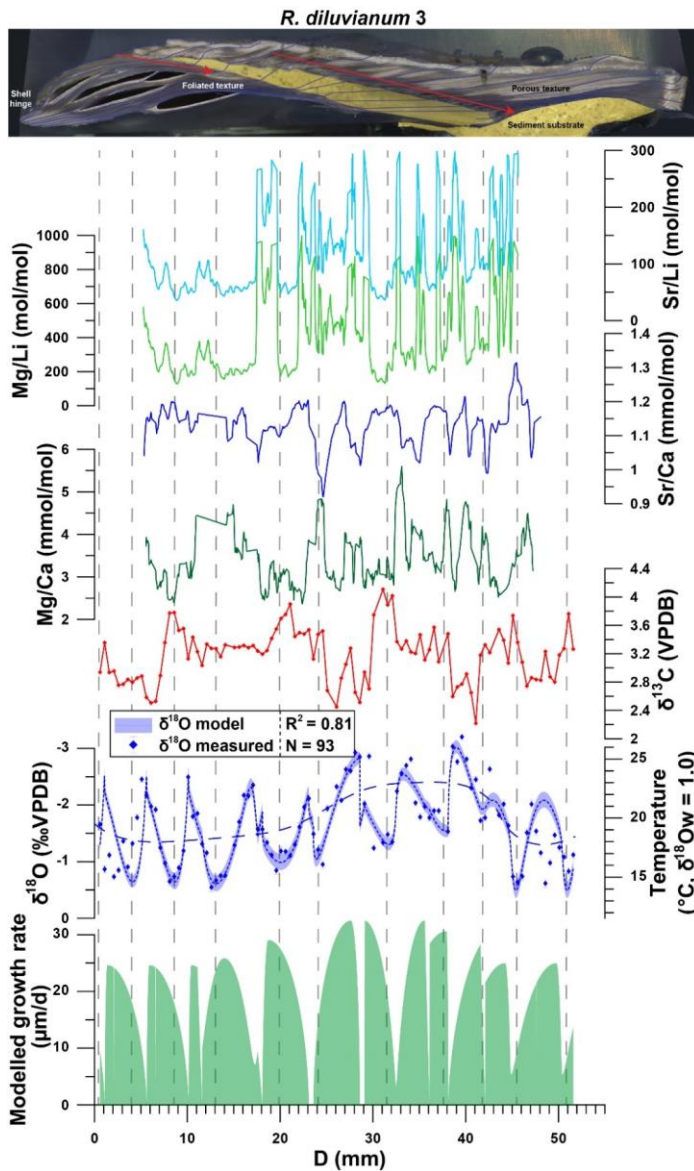


Figure 7: Example of multi-proxy records measured in *R. diluvianum* specimen 3 plotted against distance in growth direction (see image on top and **Fig. 3** for reference). From top to bottom, records of Sr/Li (light blue), Mg/Li (light green), Sr/Ca (dark blue), Mg/Ca (dark green), $\delta^{13}\text{C}$ (red), $\delta^{18}\text{O}$ (blue dots with error bars) and modelled growth rate (light green fill) are plotted. The shaded blue curve plotted underneath the $\delta^{18}\text{O}$ record illustrates the result of growth and $\delta^{18}\text{O}$ modelling and its propagated error (vertical thickness of curve, 2SD). The dashed blue curve plotted on top of the $\delta^{18}\text{O}$ record shows the observed multi-annual trend in the data. Vertical dashed lines separate growth years. Multi-proxy plots for all specimens are given in **S10**.

687 **5. Discussion**

688 **5.1 Preservation**

689 The relative lack of burial and tectonic activity in the Kristianstad Basin has provided ideal circumstances
690 for the nearly immaculate preservation of *R. diluvianum* shells in the Ivö Klack locality (Kominz et al., 2008;
691 Surlyk and Sørensen, 2010). The excellent state of these shells is evident by the preservation of original
692 (porous and foliated) microstructures that closely resemble those reported for several species of modern
693 ostreid shells (Carriker et al., 1979; Surge et al., 2001; Ullmann et al., 2010; 2013; Zimmt et al., 2018; **Fig.**
694 **2-3**). High magnification SEM images demonstrate the excellent preservation of foliated and vesicular
695 calcite structures in *R. diluvianum* shells (**Fig. 3b-d**). The preservation state of *R. diluvianum* shells meets
696 the SEM-based preservation criteria for robust stable isotope analysis set by Cochran et al. (2010).
697 MicroXRF mapping reveals that the foliated calcite in the shells is characterized by high Sr concentrations
698 and low concentrations of Mn, Fe and Si, elements which are generally associated with diagenetic alteration
699 (e.g. Brand and Veizer, 1980; Al-Aasm and Veizer, 1986a; Immenhauser et al., 2005; **Fig. 3b-h**). Trends
700 in bulk Mn and Sr concentrations observed in all fossil species from Ivö Klack (**Fig. 5b**; including less well-
701 preserved parts) likely point towards a diagenetic process affecting a less well-preserved subset of the
702 data. The lack of covariation between Mn concentration and $\delta^{18}\text{O}$ shows that there is little evidence for
703 meteoric diagenesis in these shells (**Fig. 5d**; Ullmann and Korte, 2015). Instead, these patterns are best
704 explained by early marine cementation of porous carbonate structures from sea water with similar
705 temperature and $\delta^{18}\text{O}$ as the living environment (see also Sørensen et al., 2015).

706 Typically, a Mn concentration threshold of 100 $\mu\text{g/g}$ is applied below which Cretaceous low-magnesium
707 carbonates are assumed suitable for chemical analysis (Steuber et al., 2005; Huck et al., 2011). Strontium
708 concentrations above 1000 $\mu\text{g/g}$ have also been used as markers for good preservation, since diagenetic
709 processes can cause strontium to leach out of carbonates (e.g. Brand and Veizer, 1980; Huck et al., 2011;
710 Ullmann and Korte, 2015). Previous studies of belemnites in Kristianstad Basin proposed a molar Sr/Mn
711 threshold of 100 for belemnite rostra (Sørensen et al., 2015). However, the height of thresholds used for
712 diagenetic screening differs widely in the literature due to variety-variation between species, fossil matrices
713 and burial histories (e.g. Veizer, 1983; Steuber et al., 1999; Ullmann and Korte, 2015; de Winter and Claeys,

714 2016). Applying these thresholds risks introducing biases to chemical datasets from fossil shells and may
715 not be an ideal method for diagenetic screening. Furthermore, large variation in the *in vivo* incorporation of
716 Mn and Sr in mollusk shell carbonate and a strong dependence on the diagenetic setting can make the
717 interpretation of shell preservation from trace element ratios alone highly ambiguous (Ullmann and Korte,
718 2015). The complex patterns in multi-proxy datasets in this study (**Fig. 5**) merit great care in applying simple,
719 general thresholds for grouping different processes of carbonate diagenesis. Therefore, in this study, a
720 multi-proxy approach is applied for diagenetic screening in which data is excluded based on a combination
721 of Si, Ca, Mn, Fe and Sr concentrations, $\delta^{18}\text{O}$ values as well as SEM and visual observations of the shell
722 structure at the location of measurement.

723 **5.2 Dating the Ivö Klack locality**

724 While previous attempts at dating Campanian strata mainly focused on relative dating using magneto- and
725 biostratigraphy (Montgomery et al., 1998; Jarvis et al., 2002; Voigt et al., 2010), integration of
726 cyclostratigraphic approaches ~~in this integrated stratigraphic framework~~ has recently allowed to constrain
727 the age of the Campanian deposits more precisely (Voigt and Schönfield, 2010; Thibault et al., 2012;
728 Wendler, 2013; Thibault et al. 2016). Unfortunately, these rarely cover the time interval in which the Ivö
729 Klack sediments were deposited (e.g. Wendler, 2013; Perdiou et al., 2016). Strontium isotope dating places
730 the Ivö Klack deposits at 78.14 ± 0.26 Ma (**Fig. 4**), ~~slightly above the early/late Campanian boundary. When~~
731 ~~plotting the obtained age of 78.14 Ma on the compilation by Wendler (2013), the age of the Ivö Klack falls~~
732 ~~slightly above the early/late Campanian subdivision (which is placed at 78.5 Ma),~~ while the *B. mammilatus*
733 biozone is defined as late early Campanian (Wendler, 2013). Influx of radiogenic strontium-rich weathering
734 products from the nearby Transscandinavian Igneous Belt may bias age estimates from strontium isotope
735 ratios (Högdahl et al., 2004). However, studies of modern strontium isotope ratio variability (Palmer and
736 Edmond, 1989) and the potential bias of strontium isotope ratios in shallow-water carbonates (Kuznetsov
737 et al., 2012; El Meknassi et al., 2018) show that the effect of such inputs on strontium isotope dating results
738 is generally negligible, except in semi-confined shallow-marine basins characterized by considerable
739 freshwater input and low salinities (<7 psu). No evidence exists for such exceptional conditions at Ivö Klack
740 (see 2.1). We therefore conclude that our strontium isotope age estimate, together with biostratigraphic
741 constraints, places the Ivö Klack locality in the earliest late Campanian. The refined dating of the Ivö Klack

742 deposits and fossils allows the results of sclerochronological investigations presented in this work to be
743 placed in the context of longer-term climate reconstructions with improved precision.

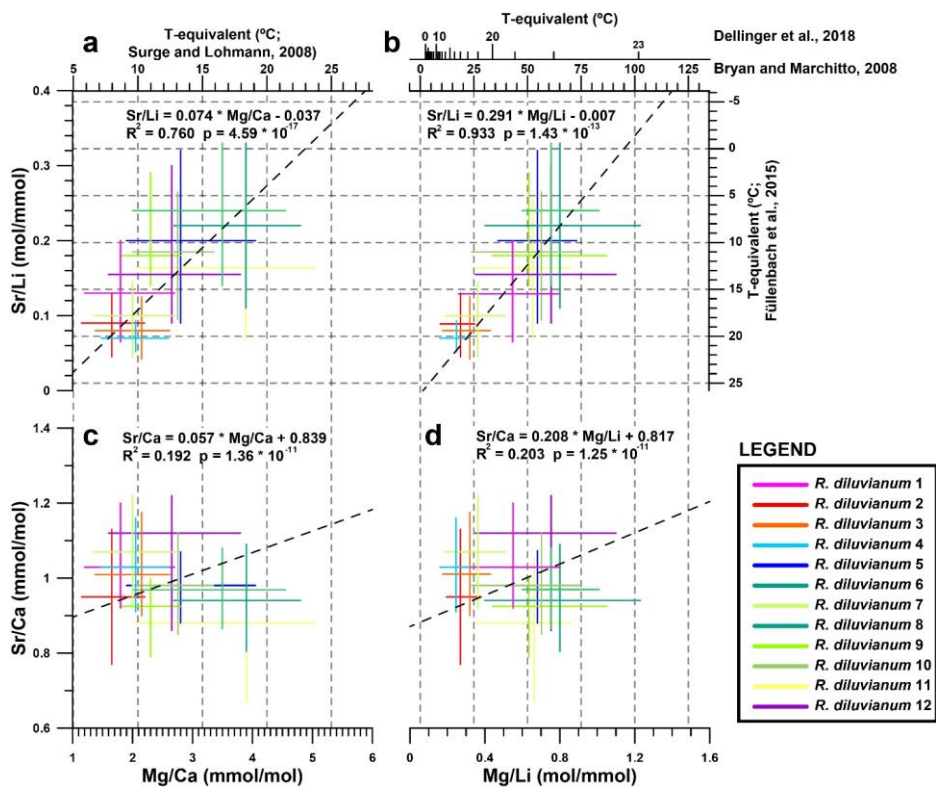
744 **5.3 Trace element variability**

745 Extracted ranges in seasonal scale periodic variability in Mg/Ca, Sr/Ca, Mg/Li and Sr/Li in all 12 *R.*
746 *diluvianum* shells (**Fig. 8**) show that it is not straightforward to interpret these records in terms of
747 temperature changes. Some of this difficulty arises from the large inter-shell variability in trace element
748 ranges, mostly expressed in strong positive correlations between Sr/Li and Mg/Ca ($R^2 = 0.76$) and between
749 Sr/Li and Mg/Li ($R^2 = 0.93$). The benthic foraminifera proxy transfer function for Mg/Li (Bryan and Marchitto,
750 2008) does not work for *R. diluvianum* (temperatures $>50^\circ\text{C}$), presumably due to typically lower Mg
751 concentrations in foraminifera compared to bivalves (Yoshimura et al., 2011). Bivalve-specific temperature
752 relationships of Mg/Ca (Surge and Lohmann, 2008; based on *Crassostrea virginica*), Sr/Li (Füllenbach et
753 al., 2015; based on *Cerastoderma edule*) and Mg/Li (Dellinger et al., 2018; based on *Mytilus edulis*) yield
754 temperatures in the same range as those reconstructed from stable oxygen isotope measurements (10-
755 20°C). However, Sr/Li-based temperature trends are opposite to those based on Mg-proxies, suggesting
756 that they cannot both be applicable to *R. diluvianum*. Poorly constrained changes in seawater chemistry
757 (Mg/Ca and Sr/Ca ratios of ocean water) also hinder these trace element-based reconstructions (Lear et
758 al., 2003; Coggron et al., 2010; Rausch et al., 2013). The strong Mg/Li-Sr/Li correlation indicates that both
759 proxies are likely strongly affected by the specimen-specific ontogenetic trends in Li/Ca described in **Table**
760 **1**. This, together with the large inter-specimen variability shows that both Li-proxies cannot be used as
761 temperature proxies in *R. diluvianum*. An annual stack of all proxies shows that the positive correlation
762 between Mg/Ca and $\delta^{18}\text{O}$ (**Fig. 9**) is opposite to the temperature-relationships found in modern oyster
763 species (Surge and Lohmann, 2008; Mouchi et al., 2013; Ullmann et al., 2013). This together with the
764 reduced seasonal variability (1.2 mmol/mol versus 4-10 mmol/mol in modern oysters; Surge and Lohmann,
765 2008; Mouchi et al., 2013) and the large (>3 mmol/mol; **Fig. 8**) inter-specimen variability both in mean value
766 and seasonal Mg/Ca range rules out Mg/Ca as a reliable temperature proxy in *R. diluvianum*. This result
767 demonstrates that earlier successful attempts to establish calibration curves for Li- and Mg-based
768 temperature proxies (e.g. Füllenbach et al., 2015; Dellinger et al., 2018) are probably strictly limited to these
769 bivalve species or close relatives. The same conclusion was also drawn by Dellinger et al. (2018) based

770 on Li/Mg and Li isotope ratio measurements in biogenic carbonates. The lack of Mg/Li or Sr/Li calibrations
771 in modern oyster shells limits the interpretation of ~~the results of this study~~ results for these element ratios.
772 Establishing such calibrations using modern oysters in cultured experiments may allow these proxies to be
773 used for reconstructions from fossil oyster shells in the future.

774 While not a likely-promising candidate for reconstructing temperature (Gillikin et al., 2005; Schöne et al.,
775 2013; Ullmann et al., 2013), seasonal Sr/Ca fluctuations and relationships between Sr/Ca and $\delta^{18}\text{O}$ are
776 consistent between individuals (**Fig. 8-9**; see also **S6**). This allows Sr/Ca ratios to be used together with
777 microstructural observations of growth increments as a basis for seasonal-scale age models in shells for
778 which no $\delta^{18}\text{O}$ measurements were done. Both mean Sr/Ca values and seasonal variability in *R. diluvianum*
779 are consistent with those observed in the same microstructure in modern *Crassostrea gigas* growing in a
780 similar environment (0.8-1.0 mmol/mol; Ullmann et al., 2013), suggesting a consistent incorporation of Sr
781 by different oyster taxa over time. It must be noted that one should be cautious when directly comparing
782 trace element concentrations in biogenic calcite between different time periods, as the seawater
783 composition of Late Cretaceous oceans (e.g. concentrations of Mg, Ca, Sr and especially Li) may have
784 been different from that of the present-day ocean (Stanley and Hardie, 1998; Coggon et al., 2010; Rausch
785 et al., 2013). Local enrichments in seawater Sr concentrations at Ivö Klack driving increased Sr ~~composition~~
786 content in *R. diluvianum* are unlikely, since Sr/Ca ratios exhibit only small (2-3%) lateral variability in the
787 world's oceans (De Villiers, 1999). Because Sr/Ca ratios in Late Cretaceous oceans were ~~twice as low as~~
788 in half those of the modern ocean, one would expect, ~~for example,~~ that Sr concentrations in Late Cretaceous
789 biogenic carbonate would be ~~twice as low as half~~ those in carbonates formed in the modern ocean, if the
790 partition coefficient between seawater concentrations and shell concentrations ~~has remains remained~~
791 constant (Stanley and Hardie, 1998; de Winter et al., 2017a). The fact that this reduction in Sr
792 concentrations relative to the modern ocean is not observed in *R. diluvianum* may ~~entail-mean~~ that there is
793 a physiologically fixed ~~physiological limit to~~ concentration of Sr in an oyster's ~~discrimination against building~~
794 Sr into their shells that is independent of ambient Sr concentrations.

795



797

798 **Figure 8:** Cross plots showing the extent of interpreted seasonality observed in records of four trace element proxies in all 12 *R.*
 799 *diluvianum* specimens. Colors of lines of individual shells correspond to colors indicated in Fig. 2. Temperature conversions from
 800 previously published regressions of the proxies with temperature are shown on opposite axes with grey dashed lines corresponding
 801 to major tick marks on the temperature scale (a) Sr/Li plotted against Mg/Ca showing a strong significant intra-shell correlation. (b)
 802 Sr/Li plotted against Mg/Li showing a strong significant intra-shell correlation due to dominant variations in Li concentration. Note that
 803 two different Mg/Li temperature calibrations were explored. (c) Sr/Ca plotted against Mg/Ca showing weak but significant intra-shell
 804 correlation. (d) Sr/Ca plotted against Mg/Li showing a weakly significant intra-shell correlation. Data for this plot is found in S13.

805

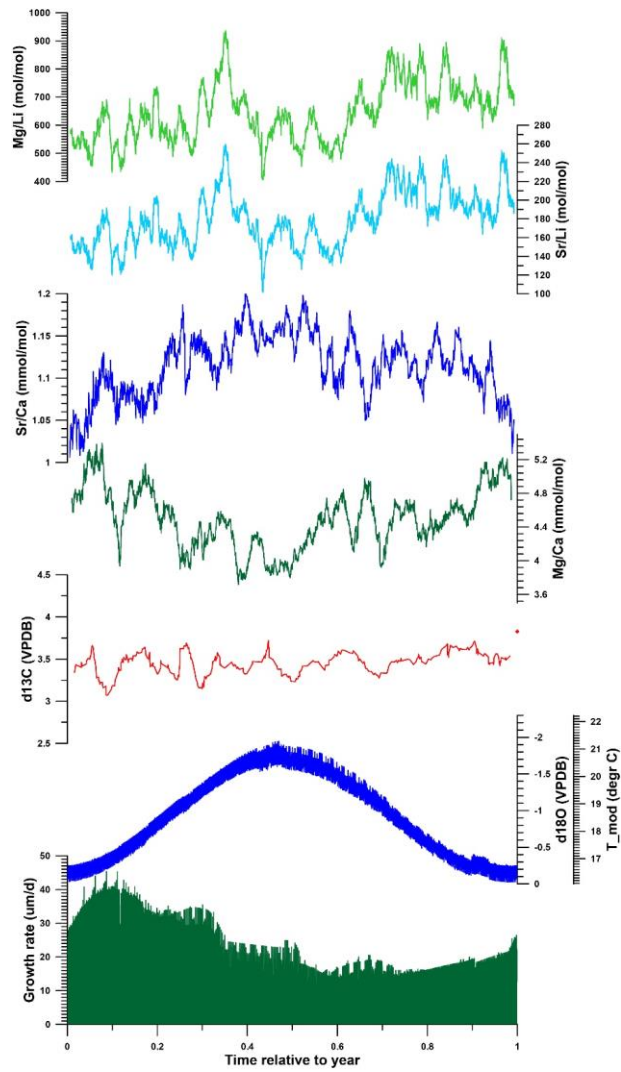


Figure 9. Composite of multi-proxy records from all *R. diluvianum* shells stacked and plotted on a common time axis of 1 year to illustrate the general phase relationships between various proxies in the shells. Records were colored as in Fig. 7. Annual stacks plotted in this figure were produced by applying age models on all multi-proxy records, plotting all results against their position relative to the annual cycle and applying 20 point moving averages.

808 5.4 Temperature seasonality

809 An annual stack of all *R. diluvianum* proxy records shows a $\delta^{18}\text{O}_c$ -based temperature variability in Ivö Klack
810 of 16-21°C when assuming a constant $\delta^{18}\text{O}_{\text{sw}}$ of -1‰VSMOW (Fig. 6). However, comparison with $\delta^{18}\text{O}$ -
811 seasonality in individual specimens shows that the annual stack severely dampens seasonality due to small
812 phase shifts in maximum and minimum temperatures, small uncertainties in the age models between years
813 and specimens, and inter-annual differences and longer-term trends in temperature (see Fig. 6). A more
814 accurate estimate of the seasonal extent is obtained by calculating the seasonal range from the coolest
815 winter temperatures (12.6°C in *R. diluvianum* 4; Fig. 6; S10) with the warmest recorded summer
816 temperature (26°C in *R. diluvianum* 1; Fig. 6; S10) which yields an extreme maximum seasonal sea surface
817 temperature (SST) range of $\pm 13.4^\circ\text{C}$.

818 A complication of these reconstructions is the assumption of constant $\delta^{18}\text{O}_{\text{sw}}$ of -1‰VSMOW, which is
819 unlikely to be completely accurate in the nearshore Ivö Klack locality. Comparison with data from
820 *Crassostrea gigas* growing in a similar nearshore environment (Ullmann et al., 2010; German North Sea
821 coast, 54°N) show that such an environment away from large river mouths can typically experience
822 seasonal salinity fluctuations of ~4 psu resulting in a dampening of the seasonal $\delta^{18}\text{O}_c$ cycle by
823 ~0.5‰VPDB. Such a salinity-effect would reduce our reconstructed 13-26°C seasonal temperature range
824 by ~2°C to 14-25°C.

825 In addition, mean annual $\delta^{18}\text{O}_{\text{sw}}$ values can be considerably ~~lighter~~lower than the global average seawater
826 composition (e.g. -1‰ to -1.5‰VSMOW compared to global ocean mean of 0‰VSMOW in Ullmann et al.,
827 2010). Considering such a deviation would reduce reconstructed temperatures by 4-6°C to 10-21°C, much
828 colder than open marine reconstructions of the Boreal Chalk Sea by Thibault et al. (2016). This result would
829 be in strong disagreement with a recent study by Tagliavento et al. (2019) in which clumped isotope
830 analyses (which ~~does~~ not rely on the assumption of constant $\delta^{18}\text{O}_{\text{sw}}$) were used to correct the $\delta^{18}\text{O}_c$ -based
831 reconstructions of the Boreal Chalk, and ~~which~~ yielded *higher* temperatures (~26°C MAT for open marine
832 SST) and a correction of $\delta^{18}\text{O}_{\text{sw}}$ towards 1-1.5‰ heavier values (resulting in a Campanian $\delta^{18}\text{O}_{\text{sw}}$ of -
833 0.5-0‰VSMOW). Another caveat is that salinity effects on local $\delta^{18}\text{O}_{\text{sw}}$ strongly depend on the local $\delta^{18}\text{O}_{\text{sw}}$
834 of the local freshwater source (riverine or precipitation), which in the present-day higher mid-latitudes is

835 around -7‰VSMOW to -8‰VSMOW (e.g. Ullmann et al., 2010), but this is impossible to constrain at Ivö
836 Klack during the Campanian within the scope of this study.

837 If local $\delta^{18}\text{O}_{\text{sw}}$ values at Ivö Klack were indeed 1-1.5‰ reduced with respect to those in the fully marine
838 Boreal Chalk Sea, and marine $\delta^{18}\text{O}_{\text{sw}}$ was around 0-0.5‰VSMOW rather than the assumed -1‰VSMOW,
839 the effects of these two biases cancel each other out, and the best estimation of the extreme seasonal SST
840 range at Ivö Klack based on this study's data would be 14-25°C with a MAT of 19°C. This MAT is
841 comparable to the MAT of the late early Campanian Boreal Chalk Sea waters of 17-19°C calculated ~~based~~
842 ~~on~~from coccolith- $\delta^{18}\text{O}_{\text{c}}$ (Lowenstam and Epstein, 1954; Jenkyns et al., 2004; Friedrich et al., 2005; Thibault
843 et al., 2016), and slightly warmer than mean annual air temperatures from this paleolatitude based on
844 phosphate- $\delta^{18}\text{O}$ reconstructions ~~paleolatitude~~ ($\pm 15^\circ\text{C}$; Amiot et al., 2004). However, Ivö Klack SST's are
845 $\sim 6^\circ\text{C}$ colder than the clumped isotope-based reconstructions from marine chalk samples (Tagliavento et
846 al., 2019). The latter could indicate that coastal SST's and air temperatures were much colder than marine
847 temperatures in the Campanian higher latitudes, but such temperature differences are highly unusual
848 compared to modern climates. Alternatively, this difference could highlight a severe temperature bias in
849 (both phosphate and carbonate) $\delta^{18}\text{O}$ -based reconstructions, which should be further investigated using
850 independent marine temperature proxies such as the clumped isotope paleothermometer (e.g. de Winter
851 et al., 2018; Tagliavento et al., 2019).

852 Modelled growth rates in *R. diluvianum* peak near the end of the low temperature season and average
853 growth rates are lowest shortly after the temperature maximum (**Fig. 9**). This phase shift between
854 temperature and growth rate could indicate that growth in *R. diluvianum* in this setting was not limited by
855 low temperatures, as observed in modern mid- to high-latitude oysters (Lartaud et al., 2010). High
856 temperature extremes ($>25^\circ\text{C}$) may have slowed or stopped growth, as recorded in modern low latitude
857 settings (Surge et al., 2001). Heat shock has been shown to limit the growth of modern oysters (*Crassostrea*
858 *gigas*; Li et al., 2007), although the relatively moderate SST seasonality suggests that ~~such~~ very high
859 ($>25^\circ\text{C}$) temperatures were not common at the Ivö Klack locality (**Fig. 6**). In this respect it is important to
860 recognise that~~In addition~~, the use of $\delta^{18}\text{O}$ records from multiple specimens reduces the effects of growth

861 cessations of individuals on seasonal SST reconstructions and allows the full seasonal range in SST to be
862 resolved.

863 The reconstructed MAT for Ivö Klack is 7-8 degrees warmer than the present-day ~~mean-annual~~seasonal
864 SST range in the North and Baltic seas at similar latitude (e.g. 2-18°C monthly seasonality range in Baltic
865 Sea Karlskrona, Sweden, 56°N and 4-18°C monthly seasonality range in North Sea Esbjerg, Denmark,
866 55°N; IRI/LDEO Climate Data Library, 2020). Seasonal SST range seasonality at Ivö Klack (11°C) is
867 significantly lower than the 14-16°C ~~temperature seasonality~~maximum seasonal range in temperature that
868 occurs in the present-day Baltic and North seas (IRI/LDEO Climate Data Library, 2020). Data on
869 temperature seasonality in the Late Cretaceous are scarce, especially in high-latitude settings. However,
870 comparison with data on Cretaceous temperature seasonality between 15°N and 35°N paleolatitude
871 (Steuber et al., 2005) shows that while MAT at 50°N was significantly lower than ~~those~~ at lower latitudes
872 (19°C ~~vs.~~and 25-30°C, respectively), the seasonal temperature range during cooler periods in the Late
873 Cretaceous was remarkably similar between latitudes (10-15°C in subtropical latitudes vs. ±14°C in this
874 study). This observation contrasts with the present-day situation in Northern Africa and Europe, in which
875 seasonal temperature ranges are generally much higher in mid- to high-latitudes (30-50°N) than in lower
876 latitudes (10-30°N; Prandle and Lane, 1995; Rayner, 2003; Locarnini et al., 2013; NOAA, 2020). Our SST
877 reconstructions also show that Late Cretaceous latitudinal temperature gradients and mid- to high-latitude
878 seasonality were larger than previously assumed based on climate model results (Barrera and Johnson,
879 1999; Hay and Floegel, 2012; Upchurch et al., 2015).

880 **5.5 Shell growth and ontogeny**

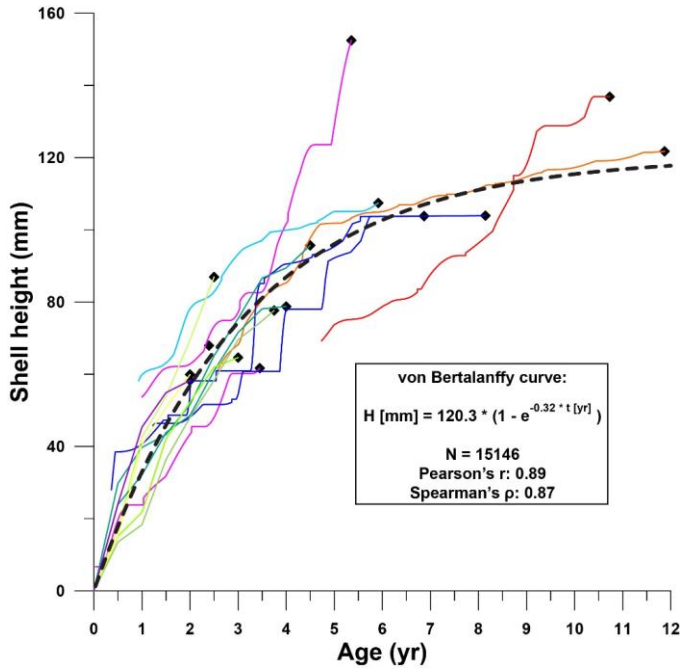
881 5.5.1. Growth curves

882 Growth curves of individual *R. diluvianum* specimens clearly converge to a general growth development
883 curve for the species (**Fig. 10**). Considering that these growth curves are based on δ¹⁸O and Sr/Ca transects
884 in different stages of life in different specimens (large age variation; see **Fig. 8**), individual growth curves
885 are remarkably similar. The growth of *R. diluvianum* takes the typical shape of the asymptotic Von
886 Bertalanffy curve, in which shell height (H_t) development with age (t) is related to a theoretical adult size
887 H_{max} and a constant k in the equation: $H_t[mm] = H_{max} * (1 - e^{k*(t[yr]-t_0)})$, with t_0 representing the time at

888 which the growth period started (always zero in this case; ~~Von-von~~ Bertalanffy, 1957). When this formula is
889 regressed over all modelled growth data of all shells (1 data point per day, 15146 points in total), the fit with
890 an H_{\max} of ± 120.3 mm and a K value of ± 0.32 is very good ($R^2 = 0.79$; see **Fig. 10**).

891 The consistency in growth curves between individuals of *R. diluvianum* is surprising as modern oyster
892 species are known to exhibit large variations in growth rates and shell shapes as a function of their colonial
893 lifestyle, which often limits the growth of their shells in several directions (Galtsoff, 1964; Palmer and
894 Carriker, 1979). The strong resemblance of growth between individuals and the close fit of the idealized
895 ~~Von-von~~ Bertalanffy growth model suggests that growth of *R. diluvianum* at Ivö Klack was relatively
896 unrestricted in space. This hypothesis is consistent with the apparent mode of life of *R. diluvianum* in Ivö
897 Klack, cemented next to each other in loose groups, subject to strong wave action and turbulence, such
898 that individuals received the same (high) supply of food but with little competition for space due to the high-
899 energy environment (Surlyk and Christensen, 1974; Sørensen et al., 2012). The shape of the growth curve
900 of *R. diluvianum* resembles that of modern Chesapeake Bay oysters (*Crassostrea virginica*), which exhibit
901 a slightly larger modelled maximum height (150 mm) and a slightly smaller K-value (0.28). A larger subset
902 of *R. diluvianum* specimens studied by Sørensen et al. (2012) demonstrates that these bivalves could grow
903 up to 160 mm in height. The curvature of the growth curve of *R. diluvianum* (K-value) is also similar to that
904 found for other modern shallow marine bivalve species (e.g. *Macoma balthica*, $K = 0.2-0.4$; Bachelet, 1980;
905 *Pinna nobilis*, $K = 0.33-0.37$; Richardson et al., 2004) and significantly higher than in growth curves of deep
906 shelf-dwelling bivalves (e.g. *Placopecten magellanicus*, $K = 0.16-0.24$; MacDonald and Thompson, 1985;
907 Hart and Chute, 2009) or bivalves from cold habitats (e.g. North Atlantic *Arctica islandica*, $K = 0.06$; Strahl
908 et al., 2007). This reflects the high growth rates (steeper growth curves, higher K-values) of shallow marine
909 bivalves compared to species living in more unfavorable or restricting less favorable (colder or deeper)
910 habitats, with *R. diluvianum* clearly being part of the former group.

911



912

913 **Figure 10:** Shell height plotted against age for all *R. diluvianum* records (see Fig. 8 for color legend of lines representing individuals).

914 The similarity between growth curves of different specimens allows a Von-von Bertalanffy curve to be fitted to the data with high

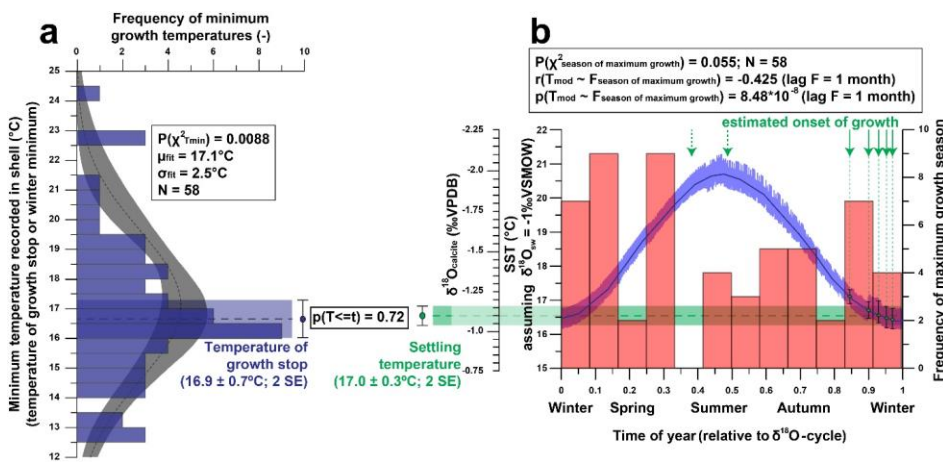
915 confidence. Sinusoidal patterns superimposed on all growth curves are caused by seasonal variability in growth rate (see Fig. 6-7).

916 Data found in S9.

917

918 5.5.2 Seasonal growth

919 To study variability in minimum growth temperature (Fig. 11a), length of the growth season and time of
 920 year ~~on-at~~ which maximum growth occurs (Fig. 11b), we isolated individual growth years from all age
 921 models of the five shells in which $\delta^{18}\text{O}$ curves were measured (Fig. 11). The onset and end of each growth
 922 year correspond to maxima in $\delta^{18}\text{O}$ values (minima in temperatures). The onset of the first growth year in
 923 each shell at its precise position relative to the seasonal temperature cycle showed in which season
 924 ~~spawning occurred~~ the individual settled and started growing its shell (Fig. 11b). All data used to create
 925 plots in Fig. 11 are provided in S14. Relationships between these growth parameters are summarized in
 926 Table 2.



927
 928 **Figure 11:** Overview of statistical evaluation of growth parameters of *R. diluvianum* derived from age modelling in shells 1-5. (a)
 929 Histogram of minimum temperatures of growth (equivalent to the time at which growth stops or the minimum yearly temperature) in
 930 *R. diluvianum* showing that the temperature ~~on-at~~ which growth slows coincides with ~~that of the spawning season~~ the time of first
 931 growth at post-larval settlement ($p = 0.717$). (b) Histogram of the season of maximum growth relative to the $\delta^{18}\text{O}$ seasonality cycle
 932 shows no significant concentration towards a favorable growing season while moments of first growth (~~spawning~~ following settlement
 933 after the larval stage) are significantly concentrated towards the ~~low~~ high- $\delta^{18}\text{O}$ season.

<i>N</i> = 58	Total annual growth (μm)	Maximum growth rate (μm/d)	Length of growth season (d)	Minimum growth temperature (°C)	Temperature seasonality (°C)	Average temperature (°C)
Temperature seasonality (°C)	R ² 0.024 p 2.16*10 ⁻¹¹	R ² 0.053 p 6.73*10 ⁻¹⁰	R ² 0.403 p 2.15*10 ⁻²²			
Average temperature (°C)	R ² 0.020 p 2.29*10 ⁻¹¹	R ² 0.027 p 6.95*10 ⁻⁷	R ² 0.008 p 2.87*10 ⁻²¹	R ² 0.565 p 3.44*10 ⁻⁷		
Age (yr)	R ² 0.000 p 1.11*10 ⁻⁹	R ² 0.062 p 9.74*10 ⁻¹²	R ² 0.002 p 1.59*10 ⁻²²	R ² 0.002 p 1.05*10 ⁻³⁰	R ² 0.059 p 4.59*10 ⁻¹	R ² 0.000 p 1.09*10 ⁻³⁵

934
935 **Table 2:** Overview of statistical evaluation of growth parameters of *R. diluvianum* derived from age modelling in shells 1-5. Coefficients
936 of determination (R²) and p-values were determined for relationships between temperature seasonality, average temperature, age of
937 the bivalve, length of the season, minimum growth temperatures and annual average and maximum growth rates. Values in green
938 indicate strong correlations while values in red indicate the absence of a correlation. Data reported in **S14**.

939 The growing season is shorter than 365 days in all but five modelled years, demonstrating that growth stops
940 or slowdowns did occur in *R. diluvianum*. Minimum growth temperatures (temperatures at which growth
941 ~~stops~~stopped) are concentrated around 17°C ($\chi^2 = 0.0088$; **Fig. 11a**) and correlate strongly to MAT
942 (R²=0.57; **Table 2**), suggesting that growth halts in *R. diluvianum* ~~are~~were not forced by an absolute
943 temperature threshold, but rather by timing relative to the seasonality (circadian rhythm). If there ~~would~~
944 ~~be~~had been a fixed temperature threshold (e.g. 6°C or 10°C for *Crassostrea gigas*; Lartaud et al., 2010;
945 Ullmann et al., 2010) the length of the growth season ~~should~~would have positively correlated with annual
946 mean temperature, but this is not the case (R²<0.1). Other authors have suggested growth in modern *C.*
947 *gigas* does not actually cease completely but rather slows down significantly, which may also have been
948 the case in *R. diluvianum*. On average, the moment of minimum growth in *R. diluvianum* occurs right after
949 the highest temperatures of the year are reached (early autumn, **Fig. 9**).

950 The ~~spawning~~season of first growth (after larval stage) is concentrated in the two last months before the
951 $\delta^{18}\text{O}$ maximum (first half of winter) when modelled water temperatures are $\pm 17^\circ\text{C}$ (**Fig. 11b**). Note that only
952 three of the five shells allowed sampling of the first month of growth, and extrapolated records for the other
953 two shells are likely unreliable. Comparing **Fig. 11a** and **Fig. 11b** shows that growth halts and ~~spawning~~
954 ~~settling~~ occur at similar temperatures ($16.9 \pm 0.7^\circ\text{C}$ and $17.0 \pm 0.3^\circ\text{C}$ respectively, $p = 0.72$), suggesting
955 that these events occur simultaneously or on either side of a seasonal growth halt (if it occurs). The timing
956 of spawning ~~and settling~~ in *R. diluvianum* differs from that in modern oysters, which generally spawn during
957 the spring season, with the young oyster spat settling in ~~in~~the summer (e.g. for *Crassostrea gigas*: Fan et
958 al., 2011). If the larval stage of *R. diluvianum* lasted as long, this would put the spawning season of *R.*

959 *diluvianum* in summer. In the case of modern oysters, it is known that reproduction requires a relatively
960 warm minimum temperatures (ideally around 22°C for *C. gigas*; Cognie et al., 2006), and that a combination
961 of salinity and temperature conditions is important (Fan et al., 2011), while extreme temperatures (>28°C;
962 Surge et al., 2001) can induce shock. ~~Perhaps the ideal~~ Similar temperature conditions occurred of at Ivö
963 Klack in summer, possibly explaining the delay of the spawning season of *R. diluvianum* are lower (~17°C)
964 or the ideal combination of temperature and salinity is met specifically in the autumn season.

965 **Figure 11b** shows that the distribution of months with fastest growth rate is random ($p(\chi^2) = 0.055$, <95%
966 confidence). However, in 27 of the 58 years, the growth peak occurs in the season with decreasing $\delta^{18}\text{O}$
967 values ("spring season"). **Table 2** shows that the extent of temperature seasonality (difference between
968 minimum and maximum $\delta^{18}\text{O}$ converted to temperature) significantly influences the length of the growing
969 season ($R^2 = 0.40$). However, total annual growth and maximum growth rates are independent of SST (both
970 seasonal extent-range and MAT) and ontogenetic age of the organism does not predict a significant part of
971 any of the above-mentioned growth and seasonality parameters (**Table 2**). If temperature controlled the
972 growth of *R. diluvianum* shells, larger temperature seasonality would increase the chance of crossing
973 thresholds of temperature tolerance which would shorten the length of the growing season. All this suggests
974 that temperature seasonality may not have been the dominant factor causing growth cessations in *R.*
975 *diluvianum*. This hypothesis is supported by the observation that temperatures at which growth cessations
976 occur ($16.9 \pm 0.7^\circ\text{C}$; **Fig. 11a**) show large variability and do not correspond significantly to the lowest
977 temperatures of the year. A possible explanation might be that these growth cessations occurred in
978 response to attempted predation or extreme weather events, which are not necessarily paced to the
979 seasonal cycle.

980 These observations do not necessarily show that *R. diluvianum* tolerated larger temperature differences
981 than modern oyster taxa, because the extent of seasonality (14-25°C) causes neither the lower (~10°C)
982 nor the upper temperature limit of temperature tolerance (~28°C) between which shell growth occurs in
983 modern oysters to be reached. If temperature tolerance of *R. diluvianum* did resemble that of its closest
984 modern relatives, then the mild seasonal temperature cycle at Ivö Klack might have provided the ideal
985 temperature range for its growth. Perhaps these favorable conditions partly explain why biodiversity and
986 abundance of invertebrates at Ivö Klack was so high (Surlyk and Sørensen, 2010).

987 5.5.3 Productivity

988 Shell growth in *R. diluvianum* may not have been governed by temperature, but rather by changes in
989 productivity. The observation that peak growth rates and ~~spawning-settling~~ both occur during the early
990 spring ~~or late autumn~~ season (~~before or after the growth cessation~~; **Fig. 11b**) supports this hypothesis.
991 Spring ~~or autumn~~ productivity blooms caused by increases in nutrient-rich freshwater from onshore (Arthur
992 et al., 1983; Krantz et al., 1987) or due to storm-induced mixing of more nutrient-rich deeper waters are
993 common in present-day mid- and high-latitude marine ecosystems (e.g. Waniek, 2003; Danielsson et al.,
994 2008). An increase in seasonal freshwater influx would cause longer growth cessations to occur in the
995 spring season, reducing the length of the growing season while also dampening the ~~reconstructed~~
996 temperature seasonality ~~reconstructed from $\delta^{18}\text{O}$ due to the influx of isotopically light fresh water which~~
997 ~~dampens the seasonal cycle~~ (see 5.5.2), ~~which~~ ~~This~~ explains the correlation found between these two
998 parameters (**Table 2**). At the same time, this freshwater input would increase reconstructed MAT by
999 increasing $\delta^{18}\text{O}$ values in *R. diluvianum* shells, explaining the weak positive correlation between MAT and
1000 length of the growing season (**Table 2**).

1001 The occurrence of spring blooms is supported by weak 0.5-1.0‰ seasonal variability in $\delta^{13}\text{C}$ (**Fig. 6**).
1002 Seasonal changes in productivity and/or salinity will cause changes in DIC in the environment, which are
1003 apparent in the $\delta^{13}\text{C}$ of the shell above the ontogenetic trends and the effect of respiration on $\delta^{13}\text{C}$ (see 2.4;
1004 **Table 1**). The fact that a clear seasonality in $\delta^{13}\text{C}$ is absent from the stack in **Fig. 9** shows that these
1005 productivity peaks do not occur at regular times of the ~~season-year~~ and that their effect on $\delta^{13}\text{C}$ is obscured
1006 by ontogenetic trends. The 0.5-1.0‰ shifts in $\delta^{13}\text{C}$ that appear to be seasonal are much smaller than those
1007 in modern oyster records (2-3‰ in low-latitude estuarine *Crassostrea virginica*; Surge et al., 2001; 2003;
1008 Surge and Lohmann, 2008). Instead, the determined shifts more closely resemble the 0.5‰ variability in
1009 $\delta^{13}\text{C}$ observed in modern *Crassostrea gigas* from the same approximate latitude as Ivö Klack in the North
1010 Sea (Ullmann et al., 2013). The extreme isotopic shifts in the estuarine *C. virginica* specimens have been
1011 shown to be caused by large shifts in freshwater input due to large seasonal variations in rainfall over
1012 southern North America (Surge et al., 2003), while smaller variations in *C. gigas* from the North Sea are
1013 produced by DIC changes due to seasonal changes in productivity (e.g. spring blooms; Ullmann et al.,

Formatted: Superscript

1014 2013), indirect effects of temperature variability (Chauvaud et al., 2011) and changes in food source
1015 (Marchais et al., 2015). The closer resemblance of *R. diluvianum* to the North Sea condition shows that the
1016 Ivö Klack paleoenvironment did not experience large seasonal shifts in freshwater input and may have seen
1017 productivity peaks in spring season. The latter interpretation is in agreement with the coincidence of
1018 negative $\delta^{13}\text{C}$ excursions (in parts of the records not affected by ontogenetic trends and respiration) with
1019 the low-high- $\delta^{18}\text{O}$ season (winter or spring; Fig. 6; S6) ~~and~~ the occurrence of spawning-settling of larvae
1020 and the onset of shell growth and a peak in growth rates in the spring season (much like in wild modern
1021 oysters; Berthelin et al., 2000; Fig. 9; Fig. 11a).

1022

1023 5.5.4 Ontogeny

1024 A part of the variation in $\delta^{13}\text{C}$ is explained by the presence of ontogenetic trends. These trends are known
1025 to occur in marine and freshwater bivalves including in bivalves with symbionts (Klein et al., 1996b;
1026 Watanabe et al., 2004; Gillikin et al., 2007; McConnaughey and Gillikin, 2008). The scale and direction of
1027 the trends in $\delta^{13}\text{C}$ are not consistent between individual *R. diluvianum* shells, which is also the case in other
1028 bivalve species (see **section 4.5; Table 1**; McConnaughey and Gillikin, 2008 and references therein).
1029 Studies of modern bivalves show that in larger (older) bivalves, the contribution of respired CO_2 to carbon
1030 in the shell is larger (up to 40%; Gillikin et al., 2007). This finding explains common trends of reducing $\delta^{13}\text{C}$
1031 with age in bivalve shells, since respired carbon is isotopically lighter than environmental DIC. Since
1032 ontogenetic trends are likely caused by changes in the amount of respired carbon entering the shell, ~~and~~
1033 but the direction of these trends is inconsistent in *R. diluvianum*, the contribution of respired CO_2 to *R.*
1034 *diluvianum* shells likely did not strictly increase with age. While this complicates the interpretation of $\delta^{13}\text{C}$
1035 records, the relative contribution of environmental changes to $\delta^{13}\text{C}$ variability in *R. diluvianum* shells does
1036 appear to be highest ~~on~~ at the positive end of the ontogenetic trend.

1037

1038 5. Conclusions

1039 The highly biodiverse marine invertebrate community at Ivö Klack in the Kristianstad Basin in southern
1040 Sweden offers a unique opportunity to recover a wealth of information about Campanian climate and
1041 environment in high latitudes and the ecology and life of extinct invertebrate species that lived under these
1042 conditions. The lack of burial and tectonic activity in the region favored *Rastellum diluvianum* fossil shells
1043 from Ivö Klack to be well preserved, as is evident from the excellent preservation of growth structures typical
1044 for ostreid shells as well as from the limited evidence for geochemical changes associated with diagenetic
1045 alteration. This excellent preservation allows the shells of *R. diluvianum* to be used to accurately and
1046 precisely constrain the age of the Ivö Klack locality using strontium isotope stratigraphy (78.14 ± 0.26 Ma;
1047 $^{87}\text{Sr}/^{86}\text{Sr} = 0.707552 \pm 0.000112$). Furthermore, *R. diluvianum* shells reveal sub-annual scale variability in
1048 temperature, local environment and growth rates through a multi-proxy geochemical approach. The
1049 combination of trace element and stable isotope measurements with growth modelling based on $\delta^{18}\text{O}$
1050 records in the shells allow all measured proxies to be aligned on the same time axis. Application of transfer
1051 functions for potential Mg/Ca, Mg/Li and Sr/Li temperature proxies established in modern invertebrates
1052 yields temperatures consistent with those calculated from $\delta^{18}\text{O}$ records. However, close examination of the
1053 seasonal phase relationships between these proxies reveals that the sub-annual variability in these trace
1054 element ratios is not controlled by temperature changes alone. This observation supports previous studies
1055 that found the expression of trace element proxies to be highly variable among species and even among
1056 different specimens of the same species. If trace element proxies are to be used for seasonality
1057 reconstructions in pre-Quaternary times, a more robust, non-species-specific model for the incorporation of
1058 trace elements by bivalves is required. Establishing such a model requires culture experiments with different
1059 bivalve species in which multiple parameters influencing trace element composition can be controlled (e.g.
1060 temperature, salinity, food intake and microstructure).

1061 Stable isotope records in *R. diluvianum* shells reveal a MAT of 19°C with a seasonal water temperature
1062 range of $\pm 11^\circ\text{C}$ (14-25°C) at Ivö Klack. This value for MAT is lower than full marine SST of Boreal Chalk
1063 recently reevaluated with the clumped isotope thermometer. The difference highlights potential biases in
1064 temperature reconstructions based on $\delta^{18}\text{O}$ values and argues for reevaluations of these proxy records
1065 with more accurate techniques such as clumped isotope analysis. Comparing the seasonal temperature
1066 range reconstructed from *R. diluvianum* shells with other Late Cretaceous seasonality records from lower

1067 latitudes reveals that both latitudinal gradients and SST seasonality outside the tropics were much higher
1068 than predicted by climate models. This disagreement between data and models clearly illustrates the
1069 ~~disadvantage of the lack of~~need for more data on Late Cretaceous seasonality outside the (sub-)tropical
1070 latitudes and highlights how important such proxy-based reconstructions are for improving our
1071 understanding of the dynamics in temperature variability in both space and time during greenhouse
1072 climates.

1073 Finally, the coupled modelling and multi-proxy approach applied in this study sheds light on the effects of
1074 environmental changes on the life cycle and sub-annual growth of *R. diluvianum* shells. This study reveals
1075 that growth curves of *R. diluvianum* strongly resemble those in modern shallow marine bivalves that grow
1076 in coastal high latitude environments. However, ontogenetic changes in growth rate of our Boreal oysters
1077 seem unrelated to temperature, in contrast to modern, high-latitude oysters that tend to lower their growth
1078 rate and cease mineralization below a certain cold threshold. We conclude that growth cessations and sub-
1079 annual changes in growth rate in *R. diluvianum* were most likely not caused by intolerable temperatures,
1080 but rather by circadian rhythm tied to the seasonal cycle and seasonal changes in sea surface productivity,
1081 driven by nutrient-rich freshwater inputs.

1082

1083 **Acknowledgements**

1084 The authors would like to thank dr. Johan Vellekoop and dr. Andrew Johnson for their review that helped
1085 improve the manuscript, as well as editor dr Aninda Mazumdar for guiding the review process. This work
1086 was made possible with help of an IWT doctoral fellowship (IWT700) and FWO postdoctoral grant
1087 (12ZB220N) awarded to Niels de Winter. Instrumentation at the VUB was funded by Hercules
1088 infrastructure grants (HERC09 and HERC46). The authors acknowledge financial and logistic support
1089 from the Flemish Research Foundation (FWO, research project G017217N) and Teledyne CETAC
1090 Technologies
1091 (Omaha, NE, USA) as well as support from VUB Strategic Research ~~(BAS48)~~. Stijn Goolaerts is funded
1092 by a Belspo Brain project (BR/175/A2/CHICXULUB). Nicolas Thibault is funded by Carlsbergfondet grant
1093 CF16-0457. The authors would like to thank David Verstraeten for his help with stable isotope analyses.

1094 We thank Bart Lippens for assisting sample preparation and Joke Belza for help with the LA-ICP-MS
1095 analyses. Thanks are due to Julien Cilis (RBINS) for his assistance with SEM imaging. The authors wish
1096 to thank Emily Judd for discussions about her growth rate model for bivalve shells and Roger Barlow for
1097 his assistance ~~with combining in handling~~ strontium isotope measurements with asymmetric error
1098 distributions.
1099

1100 **Supplementary files**

1101 All supplementary files are stored in the open access online database Zenodo and can be accessed using
1102 the following link: <https://doi.org/10.5281/zenodo.3699542>

1103

1104 **S1:** High resolution (6400 dpi) scans of cross sections through the 12 shells of *Rastellum diluvianum* used
1105 in this study.

1106 **S2:** Compilation of μ XRF maps of cross sections through the 12 shells of *Rastellum diluvianum* used in this
1107 study.

1108 **S3:** Compilation of XRF line scans measured through the foliated calcite of *Rastellum diluvianum* shells.

1109 **S4:** Compilation of LA-ICP-MS data collected within the context of this study.

1110 **S5:** Compilation of IRMS data used in this study.

1111 **S6:** Composite figures of XRF linescan data through the shells of *Rastellum diluvianum*.

1112 **S7:** Source code of the bivalve growth model adapted from Judd et al. (2018) including temperature
1113 equations for calcite.

1114 **S8:** Compilation of strontium isotope data and ages used in this study.

1115 **S9:** Compilation of the results from growth modelling on 5 *Rastellum diluvianum* shells.

1116 **S10:** Compilation figures of proxy record data plotted on time axis for all 5 shells for which modelling was
1117 carried out.

1118 **S11:** Plot of ontogenetic trends in $\delta^{13}\text{C}$ and Li/Ca proxies including statistics on the spread of the slopes of
1119 these trends.

1120 **S12:** Data on trends in $\delta^{13}\text{C}$ and Li/Ca.

1121 **S13:** Data used to create seasonality crossplots shown in **Fig. 7**.

1122 **S14:** Data on statistics of the growth rates, seasonality and spawning season of all 5 bivalves for which
1123 modelling was done.

1124

1125 **References**

1126 Al-Aasm, I. S. and Veizer, J.: Diagenetic stabilization of aragonite and low-Mg calcite, II. Stable isotopes in rudists, Journal of
1127 Sedimentary Research, 56(6), 763–770, 1986a.

1128 Al-Aasm, I. S. and Veizer, J.: Diagenetic stabilization of aragonite and low-Mg calcite, I. Trace elements in rudists, *Journal of*
1129 *Sedimentary Research*, 56(1), 138–152, 1986.

1130 Alberti, M., Fürsich, F. T., Abdelhady, A. A. and Andersen, N.: Middle to Late Jurassic equatorial seawater temperatures and
1131 latitudinal temperature gradients based on stable isotopes of brachiopods and oysters from Gebel Maghara, Egypt,
1132 *Palaeogeography, Palaeoclimatology, Palaeoecology*, 468, 301–313, doi:10.1016/j.palaeo.2016.11.052, 2017.

1133 Amiot, R., Lécuyer, C., Buffetaut, E., Fluteau, F., Legendre, S. and Martineau, F.: Latitudinal temperature gradient during the
1134 Cretaceous Upper Campanian–Middle Maastrichtian: $\delta^{18}\text{O}$ record of continental vertebrates, *Earth and Planetary Science*
1135 *Letters*, 226(1), 255–272, doi:10.1016/j.epsl.2004.07.015, 2004.

1136 Andreasson, F. P. and Schmitz, B.: Winter and summer temperatures of the early middle Eocene of France from *Turritella* \square 180
1137 profiles, , 4, 1996.

1138 Arthur, M. A., Williams, D. F. and Jones, D. S.: Seasonal temperature-salinity changes and thermocline development in the mid-
1139 Atlantic Bight as recorded by the isotopic composition of bivalves, *Geology*, 11(11), 655–659, doi:10.1130/0091-
1140 7613(1983)11<655:STCATD>2.0.CO;2, 1983.

1141 Bachelet, G.: Growth and recruitment of the tellinid bivalve *Macoma balthica* at the southern limit of its geographical distribution, the
1142 Gironde estuary (SW France), *Marine Biology*, 59(2), 105–117, 1980.

1143 Barlow, R.: Asymmetric systematic errors, arXiv preprint physics/0306138, 2003.

1144 Barrera, E. and Johnson, C. C.: Evolution of the Cretaceous Ocean-climate System, *Geological Society of America*, 1999.

1145 Berthelin, C., Kellner, K. and Mathieu, M.: Storage metabolism in the Pacific oyster (*Crassostrea gigas*) in relation to summer
1146 mortalities and reproductive cycle (West Coast of France), *Comparative Biochemistry and Physiology Part B: Biochemistry and*
1147 *Molecular Biology*, 125(3), 359–369, doi:10.1016/S0305-0491(99)00187-X, 2000.

1148 Brand, U. and Veizer, J.: Chemical diagenesis of a multicomponent carbonate system–1: Trace elements, *Journal of Sedimentary*
1149 *Research*, 50(4), 1219–1236, 1980.

1150 Brand, U. and Veizer, J.: Chemical diagenesis of a multicomponent carbonate system-2: stable isotopes, *Journal of Sedimentary*
1151 *Research*, 51(3), 987–997, 1981.

1152 Bryan, S. P. and Marchitto, T. M.: Mg/Ca–temperature proxy in benthic foraminifera: New calibrations from the Florida Straits and a
1153 hypothesis regarding Mg/Li, *Paleoceanography*, 23(2), PA2220, doi:10.1029/2007PA001553, 2008.

1154 Burgener, L., Hyland, E., Huntington, K. W., Kelson, J. R. and Sewall, J. O.: Revisiting the equable climate problem during the Late
1155 Cretaceous greenhouse using paleosol carbonate clumped isotope temperatures from the Campanian of the Western Interior
1156 Basin, USA, *Palaeogeography, Palaeoclimatology, Palaeoecology*, 516, 244–267, doi:10.1016/j.palaeo.2018.12.004, 2018.

1157 Butler, P. G., Wanamaker, A. D., Scourse, J. D., Richardson, C. A. and Reynolds, D. J.: Variability of marine climate on the North
1158 Icelandic Shelf in a 1357-year proxy archive based on growth increments in the bivalve *Arctica islandica*, *Palaeogeography,*
1159 *Palaeoclimatology, Palaeoecology*, 373, 141–151, doi:10.1016/j.palaeo.2012.01.016, 2013.

1160 Carriker, M. R., Palmer, R. E. and Prezant, R. S.: Functional ultramorphology of the dissoconch valves of the oyster *Crassostrea*
1161 *virginica*, in *Proceedings of the National Shellfisheries Association*, vol. 70, pp. 139–183. [online] Available from:
1162 https://www.researchgate.net/profile/Robert_Prezant2/publication/236964411_Functional_ultramorphology_of_the_dissoconch_valves_of_the_oyster_Crassostrea_virginica/links/53dfd2260cf2a768e49be892.pdf, 1979.

1163 Carriker, M. R., Swann, C. P., Prezant, R. S. and Counts, C. L.: Chemical elements in the aragonitic and calcitic microstructural
1164 groups of shell of the oyster *Crassostrea virginica*: A proton probe study, *Marine Biology*, 109(2), 287–297, 1991.

1165 [Chauvaud, L., Thébaud, J., Clavier, J., Lorrain, A. and Strand, Ø.: What's Hiding Behind Ontogenetic \$\delta^{13}\text{C}\$ Variations in Mollusk Shells? New Insights from the Great Scallop \(*Pecten maximus*\). *Estuaries and Coasts*, 34\(2\), 211–220, doi:10.1007/s12237-010-9267-4, 2011.](#)

1166 Christensen, W. K.: Upper Cretaceous belemnites from the Kristianstad area in Scania, Fossils and Strata., 1975.

1167 Christensen, W. K.: The Albian to Maastrichtian of southern Sweden and Bornholm, Denmark: a review, *Cretaceous Research*, 5(4),
1171 313–327, 1984.

1172 Christensen, W. K.: Paleobiogeography and migration in the Late Cretaceous belemnite family Belemnitellidae, *Acta*
1173 *palaeontologica polonica*, 42(4), 457–495, 1997.

1174 Clarke, L. J. and Jenkyns, H. C.: New oxygen isotope evidence for long-term Cretaceous climatic change in the Southern
1175 Hemisphere, *Geology*, 27(8), 699–702, 1999.

1176 Cochran, J. K., Kallenberg, K., Landman, N. H., Harries, P. J., Weinreb, D., Turekian, K. K., Beck, A. J. and Cobban, W. A.: Effect of
1177 diagenesis on the Sr, O, and C isotope composition of late Cretaceous mollusks from the Western Interior Seaway of North
1178 America, *American Journal of Science*, 310(2), 69–88, doi:10.2475/02.2010.01, 2010.

1179 Coggon, R. M., Teagle, D. A., Smith-Duque, C. E., Alt, J. C. and Cooper, M. J.: Reconstructing past seawater Mg/Ca and Sr/Ca
1180 from mid-ocean ridge flank calcium carbonate veins, *Science*, 327(5969), 1114–1117, 2010.

1181 Cognie, B., Haure, J. and Baillé, L.: Spatial distribution in a temperate coastal ecosystem of the wild stock of the farmed oyster
1182 *Crassostrea gigas* (Thunberg), *Aquaculture*, 259(1–4), 249–259, 2006.

1183 Csiki-Sava, Z., Buffetaut, E., Ósi, A., Pereda-Suberbiola, X. and Brusatte, S. L.: Island life in the Cretaceous - faunal composition,
1184 biogeography, evolution, and extinction of land-living vertebrates on the Late Cretaceous European archipelago, *Zookeys*,
1185 (469), 1–161, doi:10.3897/zookeys.469.8439, 2015.

1186 Dalbeck, P., England, J., Cusack, M., Lee, M. R. and Fallick, A. E.: Crystallography and chemistry of the calcium carbonate
1187 polymorph switch in *M. edulis* shells, *European Journal of Mineralogy*, 18(5), 601–609, doi:10.1127/0935-1221/2006/0018-0601,
1188 2006.

1189 Danielsson, VAAsa, Papush, L. and Rahm, L.: Alterations in nutrient limitations—scenarios of a changing Baltic Sea, *Journal of*
1190 *Marine Systems*, 73(3–4), 263–283, 2008.

1191 De Villiers, S.: Seawater strontium and Sr/Ca variability in the Atlantic and Pacific oceans, *Earth and Planetary Science Letters*,
1192 171(4), 623–634, 1999.

1193 DeConto, R. M., Hay, W. W., Thompson, S. L. and Bergengren, J.: Late Cretaceous climate and vegetation interactions: cold
1194 continental interior paradox, *SPECIAL PAPERS-GEOLOGICAL SOCIETY OF AMERICA*, 391–406, 1999.

1195 Dellinger, M., West, A. J., Paris, G., Adkins, J. F., von Strandmann, P. A. P., Ullmann, C. V., Eagle, R. A., Freitas, P., Bagard, M.-L.
1196 and Ries, J. B.: The Li isotope composition of marine biogenic carbonates: Patterns and Mechanisms, *Geochimica et*
1197 *Cosmochimica Acta*, 236, 315–335, 2018.

1198 Donnadieu, Y., Pucéat, E., Moiroud, M., Guillocheau, F. and Deconinck, J.-F.: A better-ventilated ocean triggered by Late
1199 Cretaceous changes in continental configuration, *Nature Communications*, 7, 10316, doi:10.1038/ncomms10316, 2016.
1200 El Meknassi, S., Dera, G., Cardone, T., De Rafélis, M., Brahmi, C. and Chavagnac, V.: Sr isotope ratios of modern carbonate shells:
1201 Good and bad news for chemostratigraphy, *Geology*, 46(11), 1003–1006, 2018.
1202 Fan, C., Koeniger, P., Wang, H. and Frechen, M.: Ligamental increments of the mid-Holocene Pacific oyster *Crassostrea gigas* are
1203 reliable independent proxies for seasonality in the western Bohai Sea, China, *Palaeogeography, palaeoclimatology,
1204 palaeoecology*, 299(3–4), 437–448, 2011.
1205 Freitas, P. S., Clarke, L. J., Kennedy, H. A. and Richardson, C. A.: Inter- and intra-specimen variability masks reliable temperature
1206 control on shell Mg/Ca ratios in laboratory and field cultured *Mytilus edulis* and *Pecten maximus* (bivalvia), *Biogeosciences
1207 Discussions*, 5(1), 531–572, 2008.
1208 Friedrich, O., Herrle, J. O. and Hemleben, C.: Climatic changes in the late Campanian—early Maastrichtian: Micropaleontological
1209 and stable isotopic evidence from an epicontinental sea, *Journal of Foraminiferal Research*, 35(3), 228–247, 2005.
1210 Friedrich, O., Herrle, J. O., Wilson, P. A., Cooper, M. J., Erbacher, J. and Hemleben, C.: Early Maastrichtian carbon cycle
1211 perturbation and cooling event: Implications from the South Atlantic Ocean, *Paleoceanography*, 24(2), PA2211,
1212 doi:10.1029/2008PA001654, 2009.
1213 Friedrich, O., Norris, R. D. and Erbacher, J.: Evolution of middle to Late Cretaceous oceans—a 55 my record of Earth’s temperature
1214 and carbon cycle, *Geology*, 40(2), 107–110, 2012.
1215 Füllenbach, C. S., Schöne, B. R. and Mertz-Kraus, R.: Strontium/lithium ratio in aragonitic shells of *Cerastoderma edule* (Bivalvia)—
1216 A new potential temperature proxy for brackish environments, *Chemical Geology*, 417, 341–355, 2015.
1217 Galtsoff, P. S.: The American Oyster: US Fish and Wildlife Service, *Fishery Bulletin*, 64, 480, 1964.
1218 Gillikin, D. P., Lorrain, A., Navez, J., Taylor, J. W., André, L., Keppens, E., Baeyens, W. and Dehairs, F.: Strong biological controls
1219 on Sr/Ca ratios in aragonitic marine bivalve shells, *Geochemistry, Geophysics, Geosystems*, 6(5), Q05009, 2005.
1220 Gillikin, D. P., Lorrain, A., Bouillon, S., Willenz, P. and Dehairs, F.: Stable carbon isotopic composition of *Mytilus edulis* shells:
1221 relation to metabolism, salinity, $\delta^{13}\text{C}$ DIC and phytoplankton, *Organic Geochemistry*, 37(10), 1371–1382, 2006.
1222 Gillikin, D. P., Lorrain, A., Meng, L. and Dehairs, F.: A large metabolic carbon contribution to the $\delta^{13}\text{C}$ record in marine aragonitic
1223 bivalve shells, *Geochimica et Cosmochimica Acta*, 71(12), 2936–2946, 2007.
1224 Hart, D. R. and Chute, A. S.: Verification of Atlantic sea scallop (*Placopecten magellanicus*) shell growth rings by tracking cohorts in
1225 fishery closed areas, *Canadian Journal of Fisheries and Aquatic Sciences*, 66(5), 751–758, 2009.
1226 Hay, W. W. and Floegel, S.: New thoughts about the Cretaceous climate and oceans, *Earth-Science Reviews*, 115(4), 262–272,
1227 2012.
1228 van Hinsbergen, D. J., de Groot, L. V., van Schaik, S. J., Spakman, W., Bijl, P. K., Sluijs, A., Langereis, C. G. and Brinkhuis, H.: A
1229 paleolatitude calculator for paleoclimate studies, *PLoS one*, 10(6), e0126946, 2015.
1230 Högdahl, K., Andersson, U. B. and Eklund, O.: The Transscandinavian Igneous Belt (TIB) in Sweden: a review of its character and
1231 evolution, *Geological survey of Finland Espoo*, 2004.
1232 Huber, B. T., Norris, R. D. and MacLeod, K. G.: Deep-sea paleotemperature record of extreme warmth during the Cretaceous,
1233 *Geology*, 30(2), 123–126, 2002.
1234 Huck, S., Heimhofer, U., Rameil, N., Bodin, S. and Immenhauser, A.: Strontium and carbon-isotope chronostratigraphy of
1235 Barremian–Aptian shoal-water carbonates: Northern Tethyan platform drowning predates OAE 1a, *Earth and Planetary Science
1236 Letters*, 304(3–4), 547–558, doi:10.1016/j.epsl.2011.02.031, 2011.
1237 Huyghe, D., Lartaud, F., Emmanuel, L., Merle, D. and Renard, M.: Palaeogene climate evolution in the Paris Basin from oxygen
1238 stable isotope ($\delta^{18}\text{O}$) compositions of marine molluscs, *Journal of the Geological Society*, 172(5), 576–587, 2015.
1239 Huyghe, D., de Rafélis, M., Ropert, M., Mouchi, V., Emmanuel, L., Renard, M. and Lartaud, F.: New insights into oyster high-
1240 resolution hinge growth patterns, *Mar Biol*, 166(4), 48, doi:10.1007/s00227-019-3496-2, 2019.
1241 Immenhauser, A., Nägler, T. F., Steuber, T. and Hippler, D.: A critical assessment of mollusk $18\text{O}/16\text{O}$, Mg/Ca, and $44\text{Ca}/40\text{Ca}$
1242 ratios as proxies for Cretaceous seawater temperature seasonality, *Palaeogeography, Palaeoclimatology, Palaeoecology*,
1243 215(3), 221–237, 2005.
1244 IPCC: IPCC, 2013: Climate Change 2013: The Physical Science Basis. Contribution of Working Group I to the Fifth Assessment
1245 Report of the Intergovernmental Panel on Climate Change, 1535 pp, Cambridge Univ. Press, Cambridge, UK, and New York.,
1246 2013.
1247 IRI/LDEO Climate Data Library URL <http://iridl.ideo.columbia.edu> (accessed 06/03/20).
1248 Ivany, L. C.: Reconstructing paleoseasonality from accretionary skeletal carbonates—challenges and opportunities, *The
1249 Paleontological Society Papers*, 18, 133–166, 2012.
1250 Ivany, L. C. and Runnegar, B.: Early Permian seasonality from bivalve $\delta^{18}\text{O}$ and implications for the oxygen isotopic composition of
1251 seawater, *Geology*, 38(11), 1027–1030, 2010.
1252 Jablonski, D., Huang, S., Roy, K. and Valentine, J. W.: Shaping the latitudinal diversity gradient: new perspectives from a synthesis
1253 of paleobiology and biogeography, *The American Naturalist*, 189(1), 1–12, 2017.
1254 Jarvis, I., Mabrouk, A., Moody, R. T. and de Cabrera, S.: Late Cretaceous (Campanian) carbon isotope events, sea-level change
1255 and correlation of the Tethyan and Boreal realms, *Palaeogeography, Palaeoclimatology, Palaeoecology*, 188(3), 215–248,
1256 2002.
1257 Jenkyns, H. C., Gale, A. S. and Corfield, R. M.: Carbon- and oxygen-isotope stratigraphy of the English Chalk and Italian Scaglia and
1258 its palaeoclimatic significance, *Geological Magazine*, 131(1), 1–34, 1994.
1259 Jenkyns, H. C., Forster, A., Schouten, S. and Damsté, J. S. S.: High temperatures in the late Cretaceous Arctic Ocean, *Nature*,
1260 432(7019), 888, 2004.
1261 Jones, D. S.: Sclerochronology: reading the record of the molluscan shell: annual growth increments in the shells of bivalve
1262 molluscs record marine climatic changes and reveal surprising longevity, *American Scientist*, 71(4), 384–391, 1983.
1263 Judd, E. J., Wilkinson, B. H. and Ivany, L. C.: The life and time of clams: Derivation of intra-annual growth rates from high-resolution
1264 oxygen isotope profiles, *Palaeogeography, Palaeoclimatology, Palaeoecology*, 490, 70–83, 2018.
1265 Kawaguchi, T. and Watabe, N.: The organic matrices of the shell of the American oyster *Crassostrea virginica* Gmelin, *Journal of
1266 Experimental Marine Biology and Ecology*, 170(1), 11–28, doi:10.1016/0022-0981(93)90126-9, 1993.

1267 Kim, S.-T. and O'Neil, J. R.: Equilibrium and nonequilibrium oxygen isotope effects in synthetic carbonates, *Geochimica et*
1268 *Cosmochimica Acta*, 61(16), 3461–3475, 1997.

1269 Klein, R. T., Lohmann, K. C. and Thayer, C. W.: Bivalve skeletons record sea-surface temperature and $\delta^{18}\text{O}$ via Mg/Ca and
1270 $^{18}\text{O}/^{16}\text{O}$ ratios, *Geology*, 24(5), 415–418, 1996a.

1271 Klein, R. T., Lohmann, K. C. and Thayer, C. W.: Sr/Ca and $^{13}\text{C}/^{12}\text{C}$ ratios in skeletal calcite of *Mytilus trossulus*: Covariation with
1272 metabolic rate, salinity, and carbon isotopic composition of seawater, *Geochimica et Cosmochimica Acta*, 60(21), 4207–4221,
1273 doi:10.1016/S0016-7037(96)00232-3, 1996b.

1274 Kominz, M. A., Browning, J. V., Miller, K. G., Sugarman, P. J., Mizintseva, S. and Scotese, C. R.: Late Cretaceous to Miocene sea-
1275 level estimates from the New Jersey and Delaware coastal plain coreholes: an error analysis, *Basin Research*, 20(2), 211–226,
1276 2008.

1277 Krantz, D. E., Williams, D. F. and Jones, D. S.: Ecological and paleoenvironmental information using stable isotope profiles from
1278 living and fossil molluscs, *Palaeogeography, Palaeoclimatology, Palaeoecology*, 58(3), 249–266, doi:10.1016/0031-
1279 0182(87)90064-2, 1987.

1280 Kuznetsov, A. B., Semikhatov, M. A. and Gorokhov, I. M.: The Sr isotope composition of the world ocean, marginal and inland seas:
1281 Implications for the Sr isotope stratigraphy, *Stratigr. Geol. Correl.*, 20(6), 501–515, doi:10.1134/S0869593812060044, 2012.

1282 Lartaud, F., Emmanuel, L., De Raféls, M., Ropert, M., Labourdette, N., Richardson, C. A. and Renard, M.: A latitudinal gradient of
1283 seasonal temperature variation recorded in oyster shells from the coastal waters of France and The Netherlands, *Facies*, 56(1),
1284 13, 2010.

1285 Lear, C. H., Elderfield, H. and Wilson, P. A.: A Cenozoic seawater Sr/Ca record from benthic foraminiferal calcite and its application
1286 in determining global weathering fluxes, *Earth and Planetary Science Letters*, 208(1), 69–84, doi:10.1016/S0012-
1287 821X(02)01156-1, 2003.

1288 Li, Y., Qin, J. G., Abbott, C. A., Li, X. and Benkendorff, K.: Synergistic impacts of heat shock and spawning on the physiology and
1289 immune health of *Crassostrea gigas*: an explanation for summer mortality in Pacific oysters, *American Journal of Physiology-*
1290 *Regulatory, Integrative and Comparative Physiology*, 293(6), R2353–R2362, 2007.

1291 Locarnini, R. A., Mishonov, A. V., Antonov, J. I., Boyer, T. P., Garcia, H. E., Baranova, O. K., Zweng, M. M., Paver, C. R., Reagan,
1292 J. R., Johnson, D. R., Hamilton, M. and Seidov, D.: World ocean atlas 2013. Volume 1, Temperature, U.S. Department of
1293 Commerce, National Oceanic and Atmospheric Administration, National Environmental Satellite, Data and Information Service,
1294 doi:10.7289/v55x26vd, 2013.

1295 Lorrain, A., Paulet, Y.-M., Chauvaud, L., Dunbar, R., Mucciarone, D. and Fontugne, M.: $\delta^{13}\text{C}$ variation in scallop shells: increasing
1296 metabolic carbon contribution with body size?, *Geochimica et Cosmochimica Acta*, 68(17), 3509–3519, 2004.

1297 Lorrain, A., Gillikin, D. P., Paulet, Y.-M., Chauvaud, L., Le Mercier, A., Navez, J. and André, L.: Strong kinetic effects on Sr/Ca ratios
1298 in the calcitic bivalve *Pecten maximus*, *Geology*, 33(12), 965–968, 2005.

1299 Lowenstam, H. A. and Epstein, S.: Paleotemperatures of the post-Aptian Cretaceous as determined by the oxygen isotope method,
1300 *The Journal of Geology*, 62(3), 207–248, 1954.

1301 MacDonald, B. A. and Thompson, R. J.: Influence of temperature and food availability on the ecological energetics of the giant
1302 scallop *Placopecten magellanicus*. I. Growth rates of shell and somatic tissue., *Marine ecology progress series*. Oldendorf,
1303 25(3), 279–294, 1985.

1304 Marchais, V., Richard, J., Jolivet, A., Flye-Sainte-Marie, J., Thébault, J., Jean, F., Richard, P., Paulet, Y.-M., Clavier, J. and
1305 Chauvaud, L.: Coupling experimental and field-based approaches to decipher carbon sources in the shell of the great scallop,
1306 *Pecten maximus* (L.). *Geochimica et Cosmochimica Acta*. 168, 58–69. doi:10.1016/j.gca.2015.07.010, 2015.

1307 McArthur, J. M., Howarth, R. J. and Bailey, T. R.: Strontium Isotope Stratigraphy: LOWESS Version 3: Best Fit to the Marine Sr-
1308 Isotope Curve for 0–509 Ma and Accompanying Look-up Table for Deriving Numerical Age, *The Journal of Geology*, 109(2),
1309 155–170, doi:10.1086/319243, 2001.

1310 McArthur, J. M., Steuber, T., Page, K. N. and Landman, N. H.: Sr-isotope stratigraphy: assigning time in the Campanian,
1311 Pliensbachian, Toarcian, and Valanginian, *The Journal of Geology*, 124(5), 569–586, 2016.

1312 McConnaughey, T. A.: Sub-equilibrium oxygen-18 and carbon-13 levels in biological carbonates: carbonate and kinetic models,
1313 *Coral Reefs*, 22(4), 316–327, 2003.

1314 McConnaughey, T. A. and Gillikin, D. P.: Carbon isotopes in mollusk shell carbonates, *Geo-Marine Letters*, 28(5–6), 287–299,
1315 doi:10.1007/s00367-008-0116-4, 2008.

1316 McConnaughey, T. A., Burdett, J., Whelan, J. F. and Paull, C. K.: Carbon isotopes in biological carbonates: respiration and
1317 photosynthesis, *Geochimica et Cosmochimica Acta*, 61(3), 611–622, 1997.

1318 Meyers, S. R. and Malinverno, A.: Proterozoic Milankovitch cycles and the history of the solar system, *PNAS*, 201717689,
1319 doi:10.1073/pnas.1717689115, 2018.

1320 Miller, K. G., Wright, J. D. and Browning, J. V.: Visions of ice sheets in a greenhouse world, *Marine Geology*, 217(3), 215–231,
1321 doi:10.1016/j.margeo.2005.02.007, 2005.

1322 Montgomery, P., Hailwood, E. A., Gale, A. S. and Burnett, J. A.: The magnetostratigraphy of Coniacian-Late Campanian chalk
1323 sequences in southern England, *Earth and Planetary Science Letters*, 156(3), 209–224, doi:10.1016/S0012-821X(98)00008-9,
1324 1998.

1325 Mook, W. G.: Paleotemperatures and chlorinities from stable carbon and oxygen isotopes in shell carbonate, *Palaeogeography,*
1326 *Palaeoclimatology, Palaeoecology*, 9(4), 245–263, doi:10.1016/0031-0182(71)90002-2, 1971.

1327 Mouchi, V., De Raféls, M., Lartaud, F., Fialin, M. and Verrecchia, E.: Chemical labelling of oyster shells used for time-calibrated
1328 high-resolution Mg/Ca ratios: a tool for estimation of past seasonal temperature variations, *Palaeogeography,*
1329 *Palaeoclimatology, Palaeoecology*, 373, 66–74, 2013.

1330 NOAA Earth System Research Laboratory: NOAA Optimum Interpolation (IO) Sea Surface Temperature (SST)
1331 <http://www.esrl.noaa.gov/psd/data/gridded/data.noaa.oisst.v2.html> (accessed 01/21/19).

1332 O'Brien, C. L., Robinson, S. A., Pancost, R. D., Sinninghe Damsté, J. S., Schouten, S., Lunt, D. J., Alsenz, H., Bornemann, A.,
1333 Bottini, C., Brassell, S. C., Farnsworth, A., Forster, A., Huber, B. T., Inglis, G. N., Jenkyns, H. C., Linnert, C., Littler, K.,
1334 Markwick, P., McAnena, A., Mutterlose, J., Naafs, B. D. A., Püttmann, W., Sluijs, A., van Helmond, N. A. G. M., Vellekoop, J.,
1335 Wagner, T. and Wrobel, N. E.: Cretaceous sea-surface temperature evolution: Constraints from TEX 86 and planktonic
1336 foraminiferal oxygen isotopes, *Earth-Science Reviews*, 172, 224–247, doi:10.1016/j.earscirev.2017.07.012, 2017.

1337 Ogg, J. G., Ogg, G. and Gradstein, F. M.: A concise geologic time scale: 2016, Elsevier., 2016.

1338 Palmer, R. E. and Carriker, M. R.: Effects of cultural conditions on morphology of the shell of the oyster *Crassostrea virginica*, in

1339 Proceedings of the National Shellfisheries Association, vol. 69, pp. 58–72., 1979.

1340 Pearson, P. N., Ditchfield, P. W., Singano, J., Harcourt-Brown, K. G., Nicholas, C. J., Olsson, R. K., Shackleton, N. J. and Hall, M.

1341 A.: Warm tropical sea surface temperatures in the Late Cretaceous and Eocene epochs, *Nature*, 413(6855), 481, 2001.

1342 Perdiou, A., Thibault, N., Anderskouv, K., Van Buchem, F., Buijs, G. J. A. and Bjerrum, C. J.: Orbital calibration of the late

1343 Campanian carbon isotope event in the North Sea, *Journal of the Geological Society*, 173(3), 504–517, 2016.

1344 Prandle, D. and Lane, A.: The annual temperature cycle in shelf seas, *Continental Shelf Research*, 15(6), 681–704,

1345 doi:10.1016/0278-4343(94)E0029-L, 1995.

1346 Rausch, S., Böhm, F., Bach, W., Klügel, A. and Eisenhauer, A.: Calcium carbonate veins in ocean crust record a threefold increase

1347 of seawater Mg/Ca in the past 30 million years, *Earth and Planetary Science Letters*, 362, 215–224, 2013.

1348 Rayner, N. A., Parker, D. E., Horton, E. B., Folland, C. K., Alexander, L. V., Rowell, D. P., Kent, E. C. and Kaplan, A.: Global

1349 analyses of sea surface temperature, sea ice, and night marine air temperature since the late nineteenth century, *Journal of*

1350 *Geophysical Research: Atmospheres*, 108(D14), doi:10.1029/2002JD002670, 2003.

1351 Reid, R. E. H.: The Chalk Sea, *The Irish Naturalists' Journal*, 17(11), 357–375, 1973.

1352 Richardson, C. A., Peharda, M., Kennedy, H., Kennedy, P. and Onofri, V.: Age, growth rate and season of recruitment of *Pinna*

1353 *nobilis* (L) in the Croatian Adriatic determined from Mg: Ca and Sr: Ca shell profiles, *Journal of Experimental Marine Biology and*

1354 *Ecology*, 299(1), 1–16, 2004.

1355 Roy, K., Jablonski, D. and Martien, K. K.: Invariant size–frequency distributions along a latitudinal gradient in marine bivalves,

1356 *PNAS*, 97(24), 13150–13155, doi:10.1073/pnas.97.24.13150, 2000.

1357 Rucker, J. B. and Valentine, J. W.: Salinity Response of Trace Element Concentration in *Crassostrea virginica*, *Nature*, 190(4781),

1358 1099–1100, doi:10.1038/1901099a0, 1961.

1359 Sano, Y., Kobayashi, S., Shirai, K., Takahata, N., Matsumoto, K., Watanabe, T., Sowa, K. and Iwai, K.: Past daily light cycle

1360 recorded in the strontium/calcium ratios of giant clam shells, *Nat Commun*, 3, 761, doi:10.1038/ncomms1763, 2012.

1361 Schöne, B. R. and Gillikin, D. P.: Unraveling environmental histories from skeletal diaries — Advances in sclerochronology,

1362 *Palaeogeography, Palaeoclimatology, Palaeoecology*, 373, 1–5, doi:10.1016/j.palaeo.2012.11.026, 2013.

1363 SCHÖNE, B. R., Houk, S. D., FREYRE CASTRO, A. D., Fiebig, J., Oschmann, W., KRÖNCKE, I., Dreyer, W. and Gosselck, F.:

1364 Daily growth rates in shells of *Arctica islandica*: assessing sub-seasonal environmental controls on a long-lived bivalve mollusk,

1365 *Palaios*, 20(1), 78–92, 2005.

1366 Schöne, B. R., Zhang, Z., Jacob, D., Gillikin, D. P., Tütken, T., Garbe-Schönberg, D., McConnaughey, T. and Soldati, A.: Effect of

1367 organic matrices on the determination of the trace element chemistry (Mg, Sr, Mg/Ca, Sr/Ca) of aragonitic bivalve shells (*Arctica*

1368 *islandica*)—Comparison of ICP-OES and LA-ICP-MS data, *Geochemical Journal*, 44(1), 23–37, 2010.

1369 Schöne, B. R., Zhang, Z., Radermacher, P., Thébault, J., Jacob, D. E., Nunn, E. V. and Maurer, A.-F.: Sr/Ca and Mg/Ca ratios of

1370 ontogenetically old, long-lived bivalve shells (*Arctica islandica*) and their function as paleotemperature proxies,

1371 *Palaeogeography, Palaeoclimatology, Palaeoecology*, 302(1), 52–64, 2011.

1372 Schöne, B. R., Radermacher, P., Zhang, Z. and Jacob, D. E.: Crystal fabrics and element impurities (Sr/Ca, Mg/Ca, and Ba/Ca) in

1373 shells of *Arctica islandica*—Implications for paleoclimate reconstructions, *Palaeogeography, Palaeoclimatology, Palaeoecology*,

1374 373, 50–59, 2013.

1375 Scotese, C.: A NEW GLOBAL TEMPERATURE CURVE FOR THE PHANEROZOIC., 2016.

1376 Shackleton, N. J.: Paleogene stable isotope events, *Palaeogeography, Palaeoclimatology, Palaeoecology*, 57(1), 91–102, 1986.

1377 Snoeck, C., Lee-Thorp, J., Schulting, R., Jong, J., Debouge, W. and Mattielli, N.: Calcined bone provides a reliable substrate for

1378 strontium isotope ratios as shown by an enrichment experiment, *Rapid communications in mass spectrometry*, 29(1), 107–114,

1379 2015.

1380 Sørensen, A. M., Surlyk, F. and Jagt, J. W. M.: Adaptive morphologies and guild structure in a high-diversity bivalve fauna from an

1381 early Campanian rocky shore, Ivö Klack (Sweden), *Cretaceous Research*, 33(1), 21–41, doi:10.1016/j.cretres.2011.07.004,

1382 2012.

1383 Sørensen, A. M., Ullmann, C. V., Thibault, N. and Korte, C.: Geochemical signatures of the early Campanian belemnite

1384 *Belemnellocamax mammillatus* from the Kristianstad Basin in Scania, Sweden, *Palaeogeography, palaeoclimatology,*

1385 *palaeoecology*, 433, 191–200, 2015.

1386 Stanley, S. M. and Hardie, L. A.: Secular oscillations in the carbonate mineralogy of reef-building and sediment-producing

1387 organisms driven by tectonically forced shifts in seawater chemistry, *Palaeogeography, Palaeoclimatology, Palaeoecology*,

1388 144(1), 3–19, 1998.

1389 Stenzel, H. B.: Aragonite and calcite as constituents of adult oyster shells, *Science*, 142(3589), 232–233, 1963.

1390 Steuber, T.: Isotopic and chemical intra-shell variations in low-Mg calcite of rudist bivalves (Mollusca-Hippuritacea): disequilibrium

1391 fractionations and late Cretaceous seasonality, *International Journal of Earth Sciences*, 88(3), 551–570, 1999.

1392 Steuber, T., Rauch, M., Masse, J.-P., Graaf, J. and Malkoč, M.: Low-latitude seasonality of Cretaceous temperatures in warm and

1393 cold episodes, *Nature*, 437(7063), 1341–1344, 2005.

1394 Strahl, J., Philipp, E., Brey, T., Broeg, K. and Abele, D.: Physiological aging in the Icelandic population of the ocean quahog *Arctica*

1395 *islandica*, *Aquatic Biology*, 1(1), 77–83, 2007.

1396 Surge, D. and Lohmann, K. C.: Evaluating Mg/Ca ratios as a temperature proxy in the estuarine oyster, *Crassostrea virginica*,

1397 *Journal of Geophysical Research: Biogeosciences*, 113(G2) [online] Available from:

1398 <http://onlinelibrary.wiley.com/doi/10.1029/2007JG000623/full> (Accessed 28 November 2016), 2008.

1399 Surge, D., Lohmann, K. C. and Dettman, D. L.: Controls on isotopic chemistry of the American oyster, *Crassostrea virginica*:

1400 implications for growth patterns, *Palaeogeography, Palaeoclimatology, Palaeoecology*, 172(3), 283–296, 2001.

1401 Surge, D. M., Lohmann, K. C. and Goodfriend, G. A.: Reconstructing estuarine conditions: oyster shells as recorders of

1402 environmental change, Southwest Florida, Estuarine, Coastal and Shelf Science, 57(5), 737–756, doi:10.1016/S0272-

1403 7714(02)00370-0, 2003.

1404 Surlyk, F. and Christensen, W. K.: Epifaunal zonation on an Upper Cretaceous rocky coast, *Geology*, 2(11), 529–534, 1974.

1405 Surlyk, F. and Sørensen, A. M.: An early Campanian rocky shore at Ivö Klack, southern Sweden, *Cretaceous Research*, 31(6), 567–

1406 576, 2010.

1407 Tagliavento, M., John, C. M. and Stemmerik, L.: Tropical temperature in the Maastrichtian Danish Basin: Data from coccolith $\Delta 47$
1408 and $\delta 18O$, *Geology*, 47(11), 1074–1078, 2019.

1409 Thibault, N., Husson, D., Harlou, R., Gardin, S., Galbrun, B., Huret, E. and Minoletti, F.: Astronomical calibration of upper
1410 Campanian–Maastrichtian carbon isotope events and calcareous plankton biostratigraphy in the Indian Ocean (ODP Hole
1411 762C): Implication for the age of the Campanian–Maastrichtian boundary, *Palaeogeography, Palaeoclimatology, Palaeoecology*,
1412 337–338, 52–71, doi:10.1016/j.palaeo.2012.03.027, 2012.

1413 Thibault, N., Harlou, R., Schovsbo, N. H., Stemmerik, L. and Surlyk, F.: Late Cretaceous (late Campanian–Maastrichtian) sea-
1414 surface temperature record of the Boreal Chalk Sea, *Climate of the Past*, 12(2), 429–438, 2016.

1415 Uchikawa, J. and Zeebe, R. E.: The effect of carbonic anhydrase on the kinetics and equilibrium of the oxygen isotope exchange in
1416 the CO₂–H₂O system: Implications for $\delta 18O$ vital effects in biogenic carbonates, *Geochimica et Cosmochimica Acta*, 95, 15–34,
1417 2012.

1418 Ullmann, C. V. and Korte, C.: Diagenetic alteration in low-Mg calcite from microfossils: a review, *Geological Quarterly*, 59(1), 3–20,
1419 2015.

1420 Ullmann, C. V., Wiechert, U. and Korte, C.: Oxygen isotope fluctuations in a modern North Sea oyster (*Crassostrea gigas*)
1421 compared with annual variations in seawater temperature: Implications for palaeoclimate studies, *Chemical Geology*, 277(1),
1422 160–166, 2010.

1423 Ullmann, C. V., Böhm, F., Rickaby, R. E., Wiechert, U. and Korte, C.: The Giant Pacific Oyster (*Crassostrea gigas*) as a modern
1424 analog for fossil ostreoids: isotopic (Ca, O, C) and elemental (Mg/Ca, Sr/Ca, Mn/Ca) proxies, *Geochemistry, Geophysics*,
1425 *Geosystems*, 14(10), 4109–4120, 2013.

1426 Upchurch Jr, G. R., Kiehl, J., Shields, C., Scherer, J. and Scotese, C.: Latitudinal temperature gradients and high-latitude
1427 temperatures during the latest Cretaceous: Congruence of geologic data and climate models, *Geology*, 43(8), 683–686, 2015.

1428 Vansteenberge, S., de Winter, N. J., Sinnesael, M., Xueqin, Z., Verheyden, S. and Claeys, P.: Benchtop μ XRF as a tool for
1429 speleothem trace elemental analysis: Validation, limitations and application on an Eemian to early Weichselian (125–97 ka)
1430 stalagmite from Belgium, *Palaeogeography, Palaeoclimatology, Palaeoecology*, 538, 109460,
1431 doi:10.1016/j.palaeo.2019.109460, 2020.

1432 Veizer, J.: Chemical diagenesis of carbonates: theory and application of trace element technique, [online] Available from:
1433 http://archives.datapages.com/data/sepm_sp/SC10/Chemical_Diagenesis.htm, 1983.

1434 Veizer, J. and Prokoph, A.: Temperatures and oxygen isotopic composition of Phanerozoic oceans, *Earth-Science Reviews*, 146,
1435 92–104, 2015.

1436 Voigt, S. and Schönfeld, J.: Cyclostratigraphy of the reference section for the Cretaceous white chalk of northern Germany,
1437 Lägerdorf–Kronsmoor: A late Campanian–early Maastrichtian orbital time scale, *Palaeogeography, Palaeoclimatology*,
1438 *Palaeoecology*, 287(1), 67–80, doi:10.1016/j.palaeo.2010.01.017, 2010.

1439 Voigt, S., Friedrich, O., Norris, R. D. and Schönfeld, J.: Campanian–Maastrichtian carbon isotope stratigraphy: shelf-ocean
1440 correlation between the European shelf sea and the tropical Pacific Ocean, *Newsletters on Stratigraphy*, 44(1), 57–72, 2010.

1441 Von Bertalanffy, L.: Quantitative laws in metabolism and growth, *The quarterly review of biology*, 32(3), 217–231, 1957.

1442 Wagnreich, M., Hohenegger, J. and Neuhuber, S.: Nannofossil biostratigraphy, strontium and carbon isotope stratigraphy,
1443 cyclostratigraphy and an astronomically calibrated duration of the Late Campanian Radotruncana calcarata Zone, *Cretaceous*
1444 *Research*, 38, 80–96, 2012.

1445 Waniek, J. J.: The role of physical forcing in initiation of spring blooms in the northeast Atlantic, *Journal of Marine Systems*, 39(1–2),
1446 57–82, 2003.

1447 Watanabe, T., Erez, J. and Müller, W.: Environmental and physiological controls on daily trace element incorporation in *Tridacna crocea*
1448 from combined laboratory culturing and ultra-high resolution LA-ICP-MS analysis, *Palaeogeography, Palaeoclimatology*,
1449 *Palaeoecology*, 496, 32–47, doi:10.1016/j.palaeo.2017.12.038, 2018.

1450 Watanabe, T., Suzuki, A., Kawahata, H., Kan, H. and Ogawa, S.: A 60-year isotopic record from a mid-Holocene fossil giant clam
1451 (*Tridacna gigas*) in the Ryukyu Islands: physiological and paleoclimatic implications, *Palaeogeography, Palaeoclimatology*,
1452 *Palaeoecology*, 212(3–4), 343–354, 2004.

1453 Weiner, S. and Dove, P. M.: An overview of biomineralization processes and the problem of the vital effect, *Reviews in mineralogy*
1454 *and geochemistry*, 54(1), 1–29, 2003.

1455 Weis, D., Kieffer, B., Maerschalk, C., Barling, J., Jong, J. de, Williams, G. A., Hanano, D., Pretorius, W., Mattioli, N., Scoates, J. S.,
1456 Goolaerts, A., Friedman, R. M. and Mahoney, J. B.: High-precision isotopic characterization of USGS reference materials by
1457 TIMS and MC-ICP-MS, *Geochemistry, Geophysics, Geosystems*, 7(8), Q08006, doi:10.1029/2006GC001283, 2006.

1458 Wendler, I.: A critical evaluation of carbon isotope stratigraphy and biostratigraphic implications for Late Cretaceous global
1459 correlation, *Earth-Science Reviews*, 126, 116–146, doi:10.1016/j.earscirev.2013.08.003, 2013.

1460 de Winter, N. J. and Claeys, P.: Micro X-ray fluorescence (μ XRF) line scanning on Cretaceous rudist bivalves: A new method for
1461 reproducible trace element profiles in bivalve calcite, edited by M. R. Petrizzo, *Sedimentology*, 64(1), 231–251,
1462 doi:10.1111/sed.12299, 2016.

1463 de Winter, N. J., Sinnesael, M., Makarona, C., Vansteenberge, S. and Claeys, P.: Trace element analyses of carbonates using
1464 portable and micro-X-ray fluorescence: performance and optimization of measurement parameters and strategies, *Journal of*
1465 *Analytical Atomic Spectrometry*, 32(6), 1211–1223, 2017b.

1466 de Winter, N. J., Goderis, S., Dehairs, F., Jagt, J. W., Fraaije, R. H., Van Malderen, S. J., Vanhaecke, F. and Claeys, P.: Tropical
1467 seasonality in the late Campanian (late Cretaceous): Comparison between multiproxy records from three bivalve taxa from
1468 Oman, *Palaeogeography, Palaeoclimatology, Palaeoecology*, 485, 740–760, 2017a.

1469 de Winter, N. J., Vellekoop, J., Vorselmans, R., Golreihani, A., Soete, J., Petersen, S. V., Casadio, S., Speijer, R. P.
1470 and Claeys, P.: An assessment of latest Cretaceous Pycnodonte vesicularis (Lamarck, 1806) shells as records for
1471 palaeoseasonality: a multi-proxy investigation, *Climate of the Past*, 14(6), 725–749, 2018.

1472 de Winter, N. J., Goderis, S., Malderen, S. J. M. V., Sinnesael, M., Vansteenberge, S., Snoeck, C., Belza, J., Vanhaecke, F. and
1473 Claeys, P.: Subdaily-Scale Chemical Variability in a *Torreites Sanchezi* Rudist Shell: Implications for Rudist Paleobiology and
1474 the Cretaceous Day-Night Cycle, *Paleoceanography and Paleoclimatology*, 35(2), e2019PA003723,
1475 doi:10.1029/2019PA003723, 2020a.

1476 de Winter, N. J., Vellekoop, J., Clark, A. J., Stassen, P., Speijer, R. P. and Claeys, P.: The giant marine gastropod *Campanile*
1477 *giganteum* (Lamarck, 1804) as a high-resolution archive of seasonality in the Eocene greenhouse world, *Geochemistry,*
1478 *Geophysics, Geosystems*, n/a(n/a), e2019GC008794, doi:10.1029/2019GC008794, 2020b.
1479 Yang, D., Huang, Y., Guo, W., Huang, Q., Ren, Y. and Wang, C.: Late Santonian-early Campanian lake-level fluctuations in the
1480 Songliao Basin, NE China and their relationship to coeval eustatic changes, *Cretaceous Research*, 92, 138–149,
1481 doi:10.1016/j.cretres.2018.07.008, 2018.
1482 Yoshimura, T., Tanimizu, M., Inoue, M., Suzuki, A., Iwasaki, N. and Kawahata, H.: Mg isotope fractionation in biogenic carbonates
1483 of deep-sea coral, benthic foraminifera, and hermatypic coral, *Anal Bioanal Chem*, 401(9), 2755, doi:10.1007/s00216-011-5264-
1484 0, 2011.
1485 Zimmt, J. B., Lockwood, R., Andrus, C. F. T. and Herbert, G. S.: Sclerochronological basis for growth band counting: A reliable
1486 technique for life-span determination of *Crassostrea virginica* from the mid-Atlantic United States, *Palaeogeography,*
1487 *Palaeoclimatology, Palaeoecology*, 516, 54–63, 2018.
1488